Journal of Hydrology 607 (2022) 127556

Contents lists available at ScienceDirect

Journal of Hydrology

journal homepage: www.elsevier.com/locate/jhydrol

Research papers

Arctic and sub-Arctic lake water δ^2H and $\delta^{18}O$ along a coastal-inland transect: Implications for interpreting water isotope proxy records

Sofia E. Kjellman [a,*], Elizabeth K. Thomas [b], Anders Schomacker [a]

[a] Department of Geosciences, UiT The Arctic University of Norway, P.O. Box 6050 Langnes, NO-9037 Tromsø, Norway
[b] Department of Geology, University at Buffalo, State University of New York, 126 Cooke Hall, Buffalo, NY 14260, USA

ARTICLE INFO

This manuscript was handled by Sally Elizabeth Thompson, Editor-in-Chief, with the assistance of Carlos Oroza, Associate Editor

Keywords:
Lake water isotopes
Precipitation isotopes
Moisture source
Evaporation
Seasonality
Proxy interpretation

ABSTRACT

High-latitude lakes are sensitive to climate change and store information about large-scale circulation changes and catchment-integrated processes. Lakes are mainly recharged by meteoric water, meaning that some lake sediment proxies may indirectly archive the stable isotopic composition of hydrogen (δ^2H) and oxygen ($\delta^{18}O$) of past precipitation. Yet, despite similar precipitation input, lakes within a region may exhibit a wide range of isotopic values due to the varying influence of inflow seasonality and evaporation. Moreover, the relative sensitivity of each lake to these controls may vary through time, something that is difficult to account for. Here, we evaluate the impact of variable inflow δ^2H and evaporation on the lake water isotopic composition across northern Fennoscandia (Norway, Finland, and Sweden). We measured lake water δ^2H and $\delta^{18}O$ of 135 lakes spanning from the north Norwegian coast along a 460 km transect to the Bothnian Bay, sampled from 2018 to 2020. Our data show that both coastal and inland lakes are sensitive to distillation during moisture transport, and that lakes farther from the Atlantic Ocean are additionally impacted by evaporation. We estimated the isotopic composition of lake water inflow values for evapo-concentrated transect lakes (δ^2H_I) using a Bayesian method. Resampled transect lakes had more depleted δ^2H_I in 2020 than in 2019, indicating either that precipitation was ^2H-depleted or that more winter precipitation contributed inflow to the lakes in 2020 compared to in 2019. We suggest that the more ^2H-depleted values in 2020 were a response to a snow-rich winter, associated with extremely positive Arctic Oscillation (AO+) conditions and increased moisture supply from the North Atlantic. We find evidence that lake water isotopic variability in this region reflects a combination of seasonal precipitation changes associated with atmospheric circulation changes, and catchment-integrated evaporation. Careful consideration of the variable sensitivity to these processes is essential when making inferences about past climate based on lake water isotope proxies.

1. Introduction

Amplified warming in the northern high latitudes is predicted to cause an intensification of the hydrological cycle (Rawlins et al., 2010; Collins et al., 2013; Bintanja & Selten, 2014; Bintanja et al., 2020). These changes affect both terrestrial and ocean freshwater budgets and have great cryospheric and ecological impact (Bring et al., 2016; Vihma et al., 2016; Wrona et al., 2016). Arctic precipitation change is caused by two main mechanisms with different seasonal imprints. Increased local evaporation mainly occurs in fall and winter, due to accelerated sea-ice loss (Bintanja & Selten, 2014; Bailey et al., 2021). In contrast, poleward moisture transport is greatest in summer, when the meridional temperature and moisture gradients increase the most and continental moisture sources play a significant role (Vázquez et al., 2016; Singh et al., 2017). Furthermore, greater interannual variability in the summer moisture influx from extrapolar regions is projected to contribute to increasing interannual variability in Arctic precipitation (Bintanja et al., 2020). The projected trends remain uncertain, relying on sparse observational data to describe complex spatiotemporal patterns. To improve the constraints on long-term variability in precipitation and atmospheric circulation, we can use lake-water-derived proxy records (Sundqvist et al., 2014; Linderholm et al., 2018).

Stable isotope ratios of oxygen ($\delta^{18}O$) and hydrogen (δ^2H) in precipitation are frequently used to infer processes in the hydrological cycle due to their sensitivity to changes in atmospheric temperature, moisture, and circulation (Dansgaard, 1964; Rozanski et al., 1993; Gat, 1996).

* Corresponding author.
E-mail addresses: sofia.e.kjellman@uit.no (S.E. Kjellman), ekthomas@buffalo.edu (E.K. Thomas), anders.schomacker@uit.no (A. Schomacker).

https://doi.org/10.1016/j.jhydrol.2022.127556
Received 12 July 2021; Received in revised form 21 January 2022; Accepted 27 January 2022
Available online 4 February 2022

Much of the variation in precipitation isotopic composition results from equilibrium fractionation during phase changes (e.g., evaporation, condensation, and freezing) during transport from the moisture source to the precipitation site (Gat, 1996). Equilibrium fractionation is highly temperature dependent, and therefore varies both spatially and temporally. The global average relationship between δ^2H and $\delta^{18}O$ in meteoric waters is described by the global meteoric water line (GMWL), defined as $\delta^2H = 8\times\delta^{18}O + 10$ (Craig, 1961). Local meteoric water lines (LMWLs) account for site-specific variation in the isotopic composition due to factors including moisture sources, transport conditions and seasonality. For example, in seasonally snowy regions, slopes of the LMWLs tend to be similar to the GMWL, but the intercepts lower than in other regions due to snow formation processes (Putman et al., 2019).

The isotopic signal of precipitation can be preserved in climate proxies, allowing us to extend our records back beyond the instrumental period. In northern Fennoscandia, the oldest temperature and precipitation amount observations date back to the 1860′s (Alexandersson, 2002), whereas precipitation isotope records are limited to a handful of sites, most of them only measuring $\delta^{18}O$, covering timespans of less than ten years each, and only after 1975 (IAEA/WMO, 2019).

Lakes are excellent archives of past climate change, as their isotopic composition often at least partially reflects precipitation isotopes, and they contain a wide range of proxies that preserve the lake water isotopic composition. In northern Fennoscandia, reconstructions of Holocene precipitation, humidity and atmospheric circulation have mainly been based on $\delta^{18}O$ from lacustrine carbonates (Hammarlund et al., 2002; Rosqvist et al., 2007), diatom biogenic silica (Shemesh et al., 2001; Rosqvist et al., 2004, 2013; Jonsson et al., 2010), and lake sediment cellulose (St. Amour et al., 2010). Other studies use δ^2H of lipid biomarkers to reconstruct different aspects of the water cycle (Nichols et al., 2009; Thienemann et al., 2019; Balascio et al., 2020).

Recent dual biomarker approaches have focused on comparing leaf waxes produced by aquatic and terrestrial plants to reconstruct Holocene and Last Interglacial atmospheric circulation changes, precipitation seasonality and summer moisture balance (Rach et al., 2017; Thomas et al., 2018, 2020; Curtin et al., 2019; Kjellman et al., 2020; Katrantsiotis et al., 2021). These approaches rely on the assumption that the aquatic plant biomarkers are minimally impacted by evaporative enrichment. This might be true for lakes in regions with positive moisture balance (precipitation > evaporation), but not for lakes in more arid areas (Cluett & Thomas, 2020).

When lakes undergo evapo-concentration, they will deviate from their starting isotopic compositions along the MWL due to kinetic fractionation, and evolve along a local evaporation line (LEL; Gat, 1996). The slope of the LEL is controlled by atmospheric conditions (e.g., temperature, relative humidity, and the isotopic composition of atmospheric moisture) and is usually between 5 and 6 at the mid-latitudes and sometimes steeper at high-latitudes (Gibson et al., 2008). If the slope of the LEL is known, it can be used, along with the lake water δ^2H and $\delta^{18}O$ values, to calculate the intersection between the LEL and the MWL, which represents lake water inflow values. One common approach to estimate regional LEL slopes is to adopt a linear regression fit to a group of lakes within the region (Clark & Fritz, 1997). This approach assumes that all the isotopic variation is a result of evaporation, and that all lakes in a region start with the same source isotopic composition (i.e., the lake inflow value; Bowen et al., 2018). This is seldom true, especially for systems with a strong seasonality. At high latitudes, the relative proportion of isotopically depleted snowfall and isotopically enriched rainfall can change between years, resulting in different inflow values from year to year (Tondu et al., 2013). Another approach is to apply theoretical modeling, based on the Craig-Gordon model, which requires knowledge of the isotopic composition of both precipitation and atmospheric moisture (Craig & Gordon, 1965), to infer inflow values for each lake individually. Regardless the technique used to calculate inflow values from evapo-concentrated lakes, most lake water δ^2H and $\delta^{18}O$ values contain information about both the degree of evaporative enrichment and the inflow isotopic composition. Thus, lake water δ^2H and $\delta^{18}O$ values can be used to infer past change in precipitation δ^2H and $\delta^{18}O$ values and evaporation, but the influence of both inflow and evaporation also confounds isotopic interpretation. Examining spatial and temporal variations in lake water δ^2H and $\delta^{18}O$ values along modern climate gradients can guide interpretations of lake water isotope proxy records.

In northern Fennoscandia, Holocene changes in lake-water-derived $\delta^{18}O$ and δ^2H are often assumed to reflect changes in North Atlantic atmospheric and oceanic circulation (e.g., Hammarlund et al., 2002; Rosqvist et al., 2007; Thienemann et al., 2019). The North Atlantic is the predominant moisture source, but during periods with a more southerly position of the polar front, precipitation can originate from Arctic air masses (Rosqvist et al., 2007). This is further complicated by the fact that Arctic and sub-Arctic lakes can display a wide range of water isotopic compositions, despite similar precipitation input (Gibson & Edwards, 2002; Jonsson et al., 2009; Cluett & Thomas, 2020). This is because meteoric water inputs are modulated by catchment characteristics and additionally modified by lake water evaporation (Leng & Marshall, 2004; Cluett & Thomas, 2020). Lake and catchment morphometry and precipitation amount control the throughflow regime of the lake, since these factors govern the lake water residence time (Jonsson et al., 2009). Furthermore, the travel time of water through surface and groundwater systems and into lakes varies in time and space depending on factors such as catchment size, slope, soil type and seasonality (Botter et al., 2010; Heidbüchel et al., 2012; Jutebring Sterte et al., 2021). Lakes with wetland-dominated catchments generally have shorter residence times and lower evaporation-to-inflow (E/I) ratios (Gibson et al., 2002). To make inferences about past climate based on changes in lake-water-derived $\delta^{18}O$ and δ^2H, we therefore need to understand both the regional climate and local hydrology (Jonsson et al., 2009; Jones et al., 2016; Cluett & Thomas, 2020).

Jonsson et al. (2009) measured the water isotopic composition of 11 lakes close to Abisko in northwestern Sweden and found that lakes in this region are mainly recharged by precipitation and shallow groundwater, with little influence of evaporation. They also demonstrated that the lake water isotopic composition varies on a seasonal basis, and that lakes with short residence time (<6 months) are more sensitive to seasonal changes, whereas lakes with longer residence times (>6 months) have lake water isotopic compositions closer to mean annual precipitation. Balascio et al. (2018) measured modern lake water isotopic composition of 15 lakes along a transect from near Tromsø in Norway to the Finnish-Swedish border. The lakes displayed decreasing isotopic values moving inland from the coast, and most of them showed little influence of evaporation. On western Greenland, a recent study of 140 lakes along an aridity gradient between the Labrador Sea and the Greenland Ice Sheet margin demonstrated that lake water $\delta^{18}O$ and δ^2H are impacted by inflow isotopic composition and catchment-integrated evaporation in all lakes, but that the relative importance of those two variables in a given lake depends on climate and lake and catchment morphometry (Cluett & Thomas, 2020).

Here, we investigate the water isotopic composition of lakes across Arctic and sub-Arctic Fennoscandia (Norway, Finland, and Sweden) to better constrain the influence of inflow isotopic composition and seasonality on the lake water isotopic composition throughout this region. We target lakes across a 460-km-long climatic gradient to explore the relative importance of inflow values and evaporative enrichment, and consider the interannual variability by comparing the isotopic composition from lakes sampled in several years. By identifying modern controls on the lake water isotopic composition, we aim to evaluate the sensitivity of lake water to changes in these hydrological and climate processes. This information is crucial to identify lakes that have the potential to accurately record the aspect of the water cycle we are interested in, and to make solid proxy interpretations.

2. Regional setting

The study area spans from the North Atlantic Ocean in the northwest to the Bothnian Bay in the southeast, between 65.74°N to 71.11°N and 18.39°E to 30.06°E (Fig. 1). The Late Weichselian Scandinavian Ice Sheet retreated from the outer coast *c.* 18–16 cal. kyr BP, whereas the interior parts were not ice-free until 11–10 cal. kyr BP (Hughes et al., 2016; Stroeven et al., 2016). The coast is characterized by alpine topography, with steep mountains intersected by subglacially eroded fjords and U-shaped valleys. The highest mountains are the Lyngen Alps, reaching up to *c.* 1800 m a.s.l. (Fig. 1b-c). The bedrock is often exposed, especially at high elevation, whereas areas closer to sea level are partly covered by Quaternary deposits (mainly till; NGU, 2021). To the southeast, the Scandinavian Mountains gradually become lower, transitioning into more gently undulating hilly terrain, reaching sea level by the Bothnian Bay (Fig. 1c). East of the Scandinavian Mountains, the till cover becomes thicker (Hirvas et al., 1988) and glaciofluvial deposits (e.g., eskers) are common (GTK, 2021).

Many of the lakes in the region owe their existence to the advances and retreats of the ice sheet and glaciers during the last glacial/interglacial cycle (Brosius et al., 2021). Lakes formed in depressions carved by the ice itself, some were dammed by glacial deposits, and still others are kettles formed due to melting of dead-ice. These processes combined resulted in a landscape with numerous lakes with diverse morphometrics. Many lakes and ponds are also associated with the minerotrophic aapa mires, characteristic for the area (Ruuhijärvi, 1983). These types of mire complexes form in flat areas with high precipitation and low evaporation (Seppä, 2002).

The water in the lakes can reflect different precipitation seasonality depending on duration of lake-ice cover, governing the amount of snowmelt bypass (i.e., how much of the snow that melts off the landscape before the lake becomes ice free; MacDonald et al., 2017). Along the Sweden-Finland border, the average duration of ice cover on the lakes (1961–2000) varies between 200 and 225 days (Laasanen, 1982; Eklund, 1999; Korhonen, 2006). Average lake freeze-up is around October 15 in northwestern Finland and November 5 in the southernmost part of the study area, whereas ice break-up occurs earlier in the south (May 18) than in the north (June 15) (Laasanen, 1982; Korhonen, 2006). In Norway, north of the Arctic Circle, the duration of ice cover on 18 lakes was monitored for periods of 7–61 years (with an average observation period of 27 years) between 1912 and 1987. Ice-cover duration varies between 175 and 220 days with a mean of 198 days. The average freeze-up date for these lakes is November 10, and the average ice break-up date is May 29 (L'Abée-Lund et al., 2021). Air temperature is the most important factor for the timing of freeze-up and break-up (Palecki & Barry, 1986; Weyhenmeyer et al., 2004), modulated by regional atmospheric circulation (Blenckner et al., 2004). Small and shallow lakes generally freeze over earlier than large and deep lakes, but lake size has less influence on the break-up dates (Korhonen, 2006).

Most of the study area lies in the middle and northern boreal zones, with areas above the tree line classified as alpine (Moen, 1998). The middle boreal zone is characterized by coniferous forest and mires, dominating the southern part of the study area and found in the lowlands along parts of the Norwegian coast. Deciduous trees are also common. The central part of the study area belongs to the northern boreal zone, characterized by birch forests, low-growing coniferous forest, and mires. In mountainous areas, the northern boreal zone transitions into tundra. The low-alpine areas are characterized by continuous cover of dwarf-shrubs and mires, whereas grasses, sedges, mosses, lichens, and forbs dominate the mid-alpine zone. At higher elevations (the high-alpine zone), the vegetation cover is sparse. Plant cover can affect runoff into lakes, and therefore the seasonal lake water inflow values (Gibson & Edwards, 2002).

The topography contributes to a strong hydroclimate gradient, with the Scandinavian Mountains acting as a barrier for air masses from the North Atlantic. The study region is located in the polar front zone, where dynamic low-pressure systems bringing warm moist air masses from the Atlantic meet dry cool air from the Arctic. The prevailing westerly winds bring the humid Atlantic air onshore, and precipitation amounts are highest along the southwestern coast due to orographic lift where the westerlies first meet the mountains (Hanssen-Bauer and Førland, 2000). Most of the moisture falls on the windward side of the mountains, sheltering the leeward side of the mountains from precipitation (Uvo, 2003). The west coast experiences mild winters and cool summers,

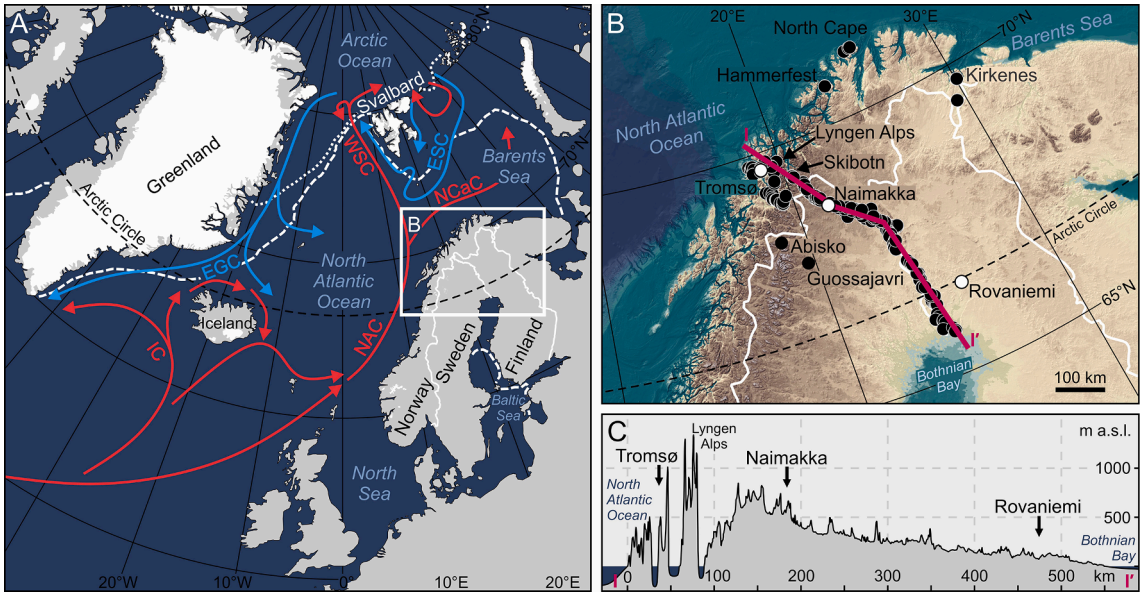

Fig. 1. (a) Overview map of the North Atlantic region, with major ocean surface currents (warm currents in red, cold in blue; NAC = North Atlantic Current; NCaC = North Cape Current; WSC = West Spitsbergen Current; IC = Irminger Current, ESC = East Spitsbergen Current; EGC = East Greenland Current), and median winter (white dashed line) and summer (white dotted line) sea-ice extent 1981–2010 (National Snow and Ice Data Center, 2019). (b) Map of the study area, showing locations of meteorological stations (white circles), sampled lakes and place names mentioned in the text (black circles) and extent of elevation profile in C (red line). Background map from IBCAO (Jakobsson et al., 2012). (c) Elevation profile from the North Atlantic Ocean in the northwest to the Bothnian Bay in the southeast. (For interpretation of the references to color in this figure legend, the reader is referred to the web version of this article.)

whereas the climate in the interior is more continental, with colder winters and warmer summers (Fig. 2a).

Seasonal variation in moisture source and moisture availability can be affected by changes in sea-ice cover. During winter (January-March), the Arctic sea ice reaches its maximum southward extent, covering the northern and eastern parts of the Barents Sea (National Snow and Ice Data Center, 2019; Fig. 1a). In winters with low sea-ice extent in the Barents Sea, more Arctic moisture can reach northern Fennoscandia (Bailey et al., 2021). Sea ice has not formed along the Norwegian coast during the Holocene (Belt et al., 2015) except in inner fjords, where it still forms today (O'Sadnick et al., 2020). Seasonal ice cover in the Bothnian Bay lasts 130–200 days, with sea ice forming in the shallow coastal areas in October–November and reaching a maximum ice extent in March (Haapala et al., 2015).

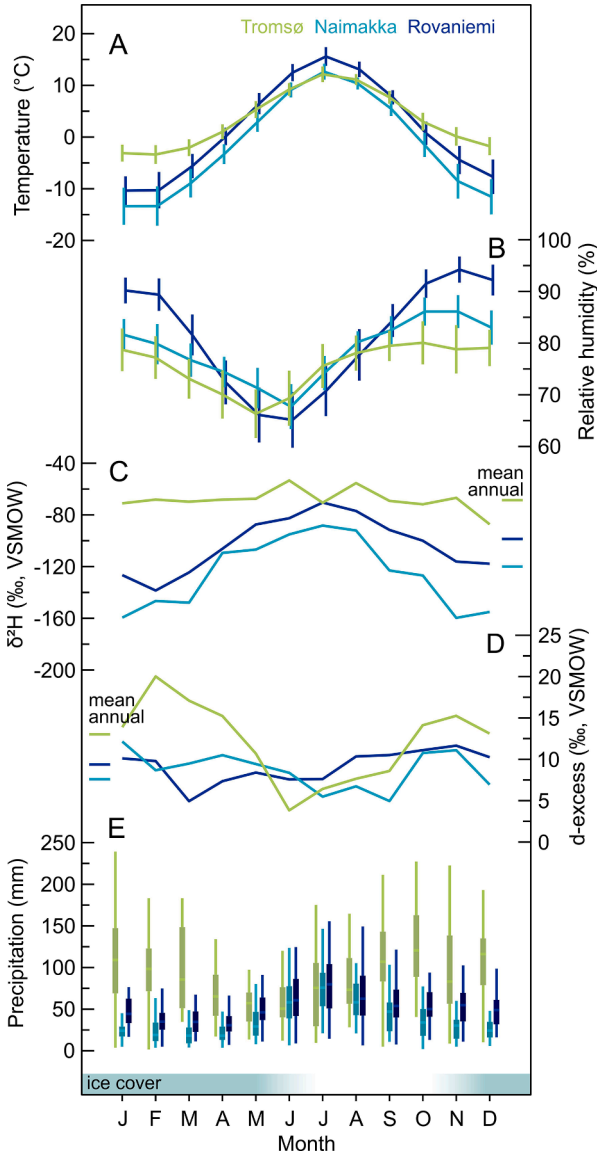

Fig. 2. Climate data from Tromsø, Naimakka and Rovaniemi (for locations, see Fig. 1). Mean monthly air temperatures (a) and relative humidity (b) between 1991-2020 (for Naimakka calculated using all months with>80% data coverage, 1995–2020). Vertical bars represent one standard deviation. (c-d) Amount-weighted monthly δ^2H and d-excess in precipitation from Tromsø (2019–2021; this study), and Naimakka (1990–1995) and Rovaniemi (2003–2014), both from IAEA/WMO (2019). (e) Monthly accumulated precipitation, 1991–2020. For each box plot, the middle line displays the median precipitation, the box represents the 25% to 75% quartile range and whiskers the maximum and minimum values. Temperature and precipitation data are retrieved from FMI (2021), MET Norway (2021) and SMHI (2021).

Winter precipitation is also strongly influenced by the North Atlantic Oscillation (NAO), controlling the strength of the westerlies (Hurrell, 1995; Uvo, 2003; Irannezhad et al., 2014). During times of positive NAO index (large atmospheric pressure difference between the Iceland Low and the Azores High), the North Atlantic storm track shifts northwards, increasing the moisture flux to Scandinavia (Hurrell, 1995; Marshall et al., 2001; Uvo, 2003). The NAO is closely related to the Arctic Oscillation (AO), which is linked to the polar low-pressure system, also known as the polar vortex (Thompson & Wallace, 1998). In the winter of 2019/2020 (January-March), which preceded one of our sampling campaigns, an exceptionally strong stratospheric polar vortex related to extreme AO+ conditions (lower than average air pressure over the Arctic and higher than average pressure over the northern Atlantic and Pacific Oceans) caused strong positive temperature (warmer) and precipitation (wetter) anomalies. The highest precipitation anomalies were observed between 60 and 70°N, greatly affecting the Norwegian coast (Lawrence et al., 2020). In contrast, some extreme snowfall events can be attributed to cold air outbreaks during strongly negative NAO and AO, when dry polar air from sea-ice covered areas moves in over a relatively warm ocean, creating large sea-air heat and moisture exchange (Shapiro et al., 1987; Papritz & Sodemann, 2018). One example of an event like this occurred in February 2018, when anomalously high temperatures and low sea-ice extent in the Barents Sea caused a high net moisture flux to the atmosphere and extreme snowfall over northern Europe (Bailey et al., 2021).

In summer, the atmospheric circulation patterns are generally not as strong, and more precipitation forms due to local convection (Jaagus, 2009). Notably, a recent Pan-Arctic study of the isotopic composition of summer 2018 rainfall identified precipitation air masses in Finland originating from two different transport regimes (Mellat et al., 2021). During NAO+ conditions, prevailing westerlies supplied Atlantic moisture, whereas summer cyclone activity related to a deepening low-pressure system over the Kara Sea caused northerly airflow and moisture transport from the Barents Sea (Mellat et al., 2021). These seasonal and synoptic changes in source impact the precipitation isotopic composition in this region (see section 2.1).

At the meteorological station in Tromsø (69.65°N, 18.94°E; 100 m a.s.l.; Fig. 1), the mean annual air temperature (MAAT, 1991–2020) is 3.3 °C and mean annual precipitation (MAP, 1991–2020) is 1091 mm (MET Norway, 2021). At the two more inland sites Naimakka (68.68°N, 21.53°E; 403 m a.s.l.) and Rovaniemi (66.50°N, 25.75°E; 107 m a.s.l.), MAAT is –1.6 °C and 1.5 °C, and MAP 466 mm and 633 mm, respectively (FMI, 2021; SMHI, 2021). Naimakka is the most continental (coldest and driest) of these sites, located on the eastern side of the Scandinavian Mountains (Fig. 1). Rovaniemi is farther from the North Atlantic Ocean, but experiences a warmer and wetter climate than Naimakka, perhaps due to its proximity to the Bothnian Bay. Significant differences in precipitation amount between the coastal and inland sites occur in fall and winter (Fig. 2e). This is the season when the relative temperature difference between (warm) ocean and (cold) land is greatest, causing high precipitation amounts at coastal locations such as Tromsø. In Rovaniemi and Naimakka, the relative humidity is high during the fall and winter months (Fig. 2b), and most precipitation falls during the warm months (Fig. 2e).

2.1. Isotopic setting

Northern Fennoscandia receives moisture from sources with different isotopic composition, where Arctic and Baltic sea surface waters are relatively depleted compared to the predominant North Atlantic source region, and the western Barents Sea (LeGrande & Schmidt, 2006; Bonne et al., 2019). In our study area, precipitation δ^2H and $\delta^{18}O$ have been monitored in Naimakka (1990–1995) and Rovaniemi (2003–2014) as part of the Global Network of Isotopes in Precipitation (GNIP; IAEA/

WMO, 2019; Fig. 1b). These data yield LMWLs with the equations $\delta^2H = 7.61\times\delta^{18}O + 2.59$ (Naimakka) and $\delta^2H = 7.70\times\delta^{18}O + 5.01$ (Rovaniemi; Fig. 3), having slightly lower slopes than the GMWL and lower intercepts. Precipitation is most depleted at Naimakka, where amount-weighted mean annual precipitation δ^2H and $\delta^{18}O$ are –119.94‰ and –16.04‰, respectively (Figs. 2 and 3). The mean isotopic composition of precipitation δ^2H and $\delta^{18}O$ during the ice-free season (June-October) are –102.38‰ and –13.70‰, and during the ice-cover season (November-May) –144.14‰ and –19.40‰. In Rovaniemi, amount-weighted mean annual precipitation δ^2H and $\delta^{18}O$ are –98.56‰ and –13.52‰, whereas ice-free season mean values are –83.31‰ and –11.59‰ and ice-cover season mean values –113.43‰ and –15.35‰, respectively. The amount-weighted mean annual values in Rovaniemi are close to Naimakka mean summer (ice-free season) values, and 21.38‰ (δ^2H) and 2.52‰ ($\delta^{18}O$) enriched compared to Naimakka amount-weighted annual values.

For regions with no GNIP stations nearby, interpolated precipitation isotope values can be generated using the Online Isotopes in Precipitation Calculator (OIPC; Bowen, 2021). However, these values can be biased towards the closest GNIP station values, not capturing local variability. Balascio et al. (2018) noted that water from lakes close to Tromsø was significantly enriched compared to both annual and summer OIPC estimations, indicating that the OIPC generates too depleted values for Tromsø, located at lower elevation and more coastal than the nearest GNIP stations. To evaluate the modern isotopic range of precipitation by the coast, we analyzed precipitation samples collected in Tromsø (69.68°N, 18.96°E; 73 m a.s.l.) between September 6, 2019, and September 5, 2021 (n = 407). These data yield a LMWL with the equation $\delta^2H = 6.68\times\delta^{18}O - 0.85$, having a lower slope and intercept than Rovaniemi and Naimakka (Fig. 3). The amount-weighted mean annual precipitation δ^2H and $\delta^{18}O$ values in Tromsø are –68.61‰ and –10.20‰, respectively (Figs. 2 and 3). This is 42.39‰ and 4.70‰ enriched compared to the OIPC estimated mean annual values (–111‰ and –14.9‰) for δ^2H and $\delta^{18}O$ at this site, respectively (Bowen, 2021). The mean annual precipitation values in Tromsø are 29.95‰ and 51.33‰ (^2H) and 3.32‰ and 5.84‰ (^{18}O) enriched compared to Rovaniemi and Naimakka, respectively. Mean ice-free season precipitation δ^2H and $\delta^{18}O$ values in Tromsø are –65.23‰ and –9.19‰, and ice-cover season mean values are –70.63‰ and –10.81‰ (Fig. 3).

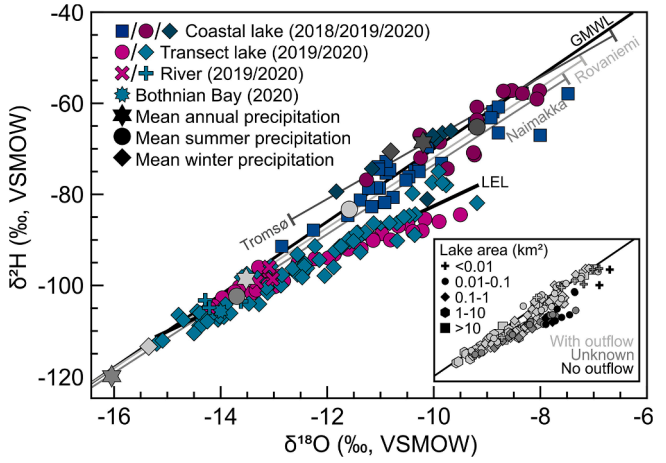

Fig. 3. $\delta^{18}O$ versus δ^2H values for all lakes and rivers sampled from 2018 to 2020, plotted against the global meteoric water line (GMWL, $\delta^2H = 8\times\delta^{18}O + 10$) and local meteoric water lines (LMWLs) from Tromsø ($\delta^2H = 6.68\times\delta^{18}O - 0.85$), Naimakka ($\delta^2H = 7.61\times\delta^{18}O + 2.59$) and Rovaniemi ($\delta^2H = 7.70\times\delta^{18}O + 5.01$). Amount-weighted mean annual, mean ice-cover (November-May = winter) and mean ice-free season (June-October = summer) precipitation are displayed for the three stations in grey. Mean ice-cover season precipitation $\delta^{18}O$ and δ^2H for Naimakka are too depleted (–19.40‰ and –144.14‰, respectively) to be displayed in the plot. Local evaporation line (LEL) is included for the transect lakes ($\delta^2H = 5.50\times\delta^{18}O - 27.55$). Inset panel has the same axes as the main figure and shows values by lake size (symbol) and throughflow regime (color).

3. Materials and methods

3.1. Water sample collection and isotope analysis

We collected lake water samples from a total of 135 lakes in northern Norway, Finland, and Sweden (Fig. 1, Supplementary Information) between 2018 and 2020. Most of the samples were collected during the first week of July, in 2018, 2019 and 2020. This is after the snowmelt season, although some high elevation lakes are fed by snowmelt throughout summer. In July 2018, we sampled lakes in the coastal Tromsø area (n = 30), and at the end of June 2019 along the north Norwegian coast (n = 9). The July 2019 and 2020 field campaigns targeted lakes (n = 35 and n = 68, respectively) along a NW-SE transect from southeast of the Lyngen Alps to the Bothnian Bay (hereafter referred to as the 'transect lakes'), between 69.4°N, 20.3°E and 65.7°N, 24.6°E (Fig. 1b–c). This transect spans *c.* 460 km, with lakes spanning elevations from close to sea level in NW and SE, up to *c.* 560 m a.s.l. close to the tripoint between Norway, Finland, and Sweden (Fig. 1c). We also collected samples from the Muonio and Torne Rivers (two rivers forming the border between Sweden and Finland) and the Bothnian Bay. To evaluate the interannual variability, we sampled 12 of the lakes along the transect and two locations on the Muonio River for two consecutive years. Furthermore, 11 of the transect lakes were sampled in July 2013 by Balascio et al. (2018), and five have been sampled all three years (2013, 2019 and 2020). Additionally, a couple of the coastal lakes were resampled in July 2019 and 2020 (n = 2 and n = 4, respectively) and/or during other times of the year (n = 5; Supplementary Information). Two coastal lakes were sampled for the first time in 2020. We collected the samples from the shoreline, approximately 10 cm below the lake surface to avoid evaporatively enriched water and stored them in 4 mL glass vials with no headspace. The vials were sealed with Parafilm to prevent evaporation during transportation and storage.

Precipitation samples were collected in Tromsø (69.68°N, 18.96°E; 73 m a.s.l.) from September 6, 2019, to September 5, 2021 (n = 407). Samples were collected each morning, using a 4-inch diameter RG202 Stratus All-Weather Rain Gauge. Liquid precipitation was collected using a funnel and an inner 1-inch cylinder, and solid precipitation from the 4-inch cylinder. The samples were transferred to 4 mL glass vials, sealed with Parafilm, and kept at 4 °C until analysis. Frozen samples were brought inside and melted in a sealed container at room temperature before transfer. Prior to analysis, all samples (lake water and precipitation) were filtered through a 0.2-μm PTFE filter.

The lake water samples collected in 2018 and 2019 were measured on a Picarro L2130-i WS-CRDS analyzer with vaporization module V1102-i coupled to a CTC PAL autosampler, at the Organic and Stable Isotope Biogeochemistry Laboratory at the University at Buffalo, USA. Each sample was measured four times, and the first injection discarded. Reported values are the average of the last three measurements. Calibration to the VSMOW scale was done using three in-house standards, spanning a range of –265.86 to + 21.43‰ for δ^2H and –33.62 to + 12.41‰ for $\delta^{18}O$, calibrated against primary standards (GISP, VSMOW2, and SLAP2) from the International Atomic Energy Agency (IAEA). A memory correction was applied, following van Geldern & Barth (2012). Average standard deviations of replicate measurements were 0.08‰ and 0.02‰ for δ^2H and $\delta^{18}O$, respectively. For lake water samples collected in 2020, and for all precipitation samples, δ^2H and $\delta^{18}O$ were measured on a Picarro L2140-i WS-CRDS with a A0211 vaporizer and an A0325 autosampler at the Facility for advanced isotopic research and monitoring of weather, climate, and biogeochemical cycling (FARLAB), University of Bergen, Norway. Each sample was measured 12 times, and the reported values are averaged over the last four to six injections. Calibration was done using a drift standard and two laboratory

standards, spanning a range of –308.14 to + 9.2‰ for δ^2H and –40.06 to + 1.77‰ for $\delta^{18}O$, calibrated against VSMOW2 and SLAP2. To reduce memory effects, a 2-component memory correction was applied, following Gröning (2011). Average standard uncertainties for calibrated measurement values (provided according to Gröning, 2018) were 0.43‰ and 0.06‰ for δ^2H and $\delta^{18}O$, respectively.

Isotope ratios are reported in per mil (‰) relative to Vienna Standard Mean Ocean Water (VSMOW), where $\delta = 1000\times((R_{sample}/R_{VSMOW}) - 1)$ and R is the ratio between $^2H/^1H$ or $^{18}O/^{16}O$. Deuterium excess (d-excess) was calculated as d-excess $= \delta^2H - 8\times\delta^{18}O$ (Dansgaard, 1964). The daily precipitation data were converted into monthly amount-weighted mean values using the equation $\delta_{aw} = \frac{1}{P}\times\sum_{i=1}^{n}(p_i\times\delta_i)$, where P and p_i are the monthly and daily precipitation amounts (in mm), δ_i is δ^2H or $\delta^{18}O$ and n is the number of sampling days.

3.2. Inferring inflow δ^2H values

To estimate lake inflow δ^2H and $\delta^{18}O$ values for the evapo-concentrated transect lakes, we applied the Bayesian 'MWL source implementation' method by Bowen et al. (2018). This method allows the user to supply a MWL equation and a hypothesized LEL slope, each with confidence intervals. Since the LMWLs in Naimakka and Rovaniemi are parallel to and have similar intercepts as the GMWL (Fig. 3), we used the default MWL equation provided with the model, which is a re-calibrated GMWL ($\delta^2H = 8.01\times\delta^{18}O + 9.57$; $n = 80{,}672$; Bowen et al., 2018). The GMWL has much less uncertainty than the LMWLs, which are constrained by only hundreds of data points. To allow for interannual comparison, we based the LEL estimations on linear regression using the isotopic composition of lakes sampled in both 2019 and 2020 ($n = 12$). To run the model, we supplied the estimated LEL slope for each subset (4.82 and 5.18 for 2019 and 2020, respectively) with a standard deviation of 0.5 (as suggested by Bowen et al., 2018), lake water δ^2H and $\delta^{18}O$ with uncertainties and covariance (0.95), and the number of iterations (10,000). We acknowledge the assumptions involved in a regression-based approach for LEL slope estimation, but consider the supplied LEL slopes to be a good starting estimate, because they agree with theoretical LEL slope values (~5) modeled by Gibson et al. (2008). Given uncertainties in the LEL regression approach, we do not interpret interannual or spatial differences in LELs, and instead use them as a guide to infer whether lakes have experienced evaporative enrichment. We present modeled mean source water values, hereafter referred to as inferred inflow δ^2H (δ^2H_I). For the discussion where we compare the seasonality of inflow between coastal and transect lakes, we include only the coastal lakes that are through-flowing, as lake water δ^2H (δ^2H_L) in these lakes is not significantly affected by evaporative enrichment, and therefore equal to δ^2H_I. We exclude small isolated coastal basins, since we do not have a well-constrained estimate of the LEL by the coast.

4. Results

4.1. Lake water isotopic composition

The lake water surface samples from 2018 to 2020 span a broad range of isotopic compositions (Fig. 3). Generally, lakes close to the

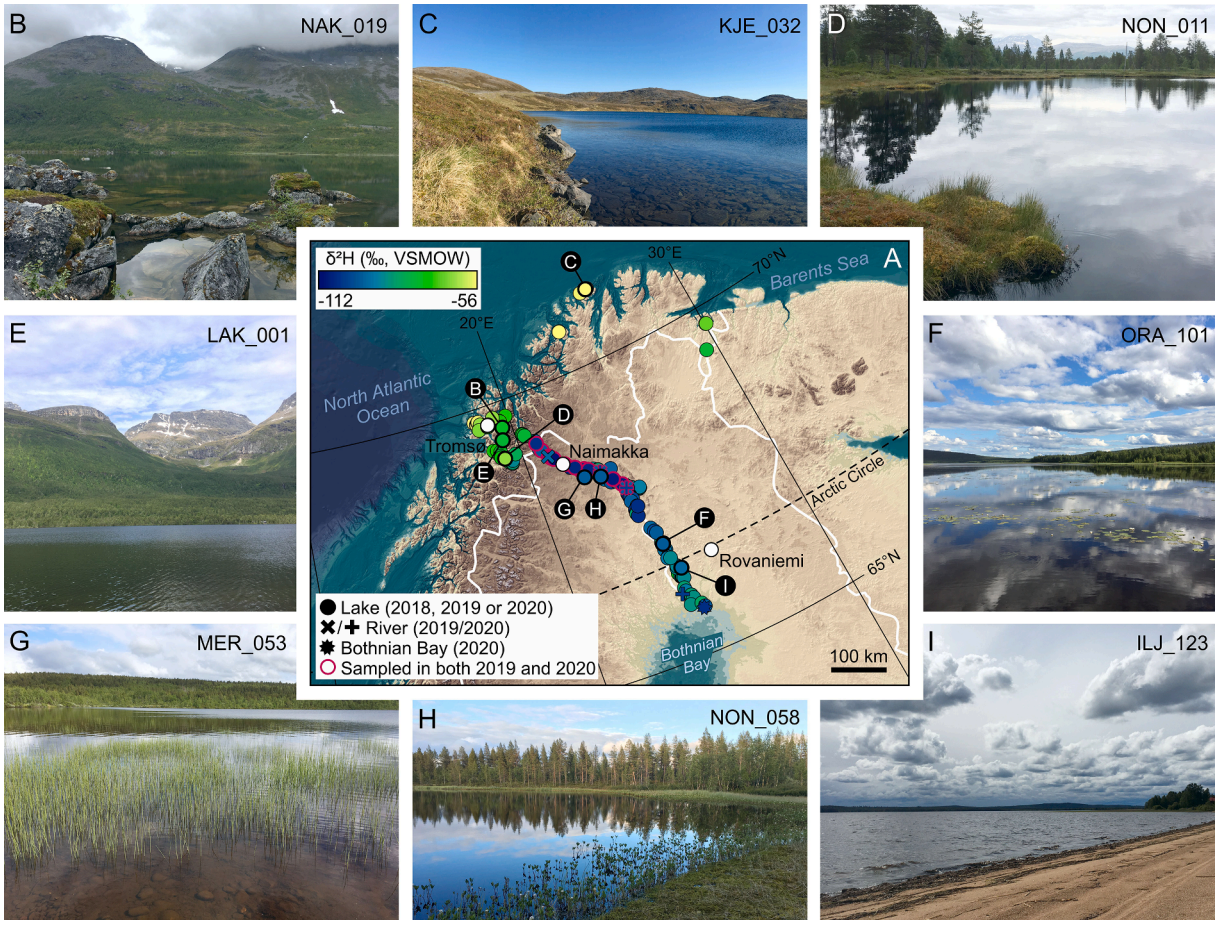

Fig. 4. (a) Geographical distribution of surface water δ^2H for 135 lakes, two rivers and the Bothnian Bay, in Arctic and sub-Arctic Norway, Finland, and Sweden. Twelve lakes and two locations along the Muonio River sampled in both 2019 and 2020 are outlined in red. Background map from IBCAO (Jakobsson et al., 2012). (b-i) Photographs of a selection of the sampled lakes. Codes refer to lake IDs (Supplementary Information). (For interpretation of the references to color in this figure legend, the reader is referred to the web version of this article.)

Norwegian (Atlantic) coast lie on or close to the GMWL, with a trend toward more ^{2}H-depleted values moving inland (Figs. 4–7). This trend is likely controlled by the increasing distance from the coast, which is likely a proxy for the degree of distillation resulting from air masses advecting over the mountain peaks (Fig. 5a and 7). The lake elevation, which is often below the highest mountain peaks in the region (Fig. 5b), is less important than the elevation of the mountains over which the moisture has to pass along its transport path (Fig. 7). In the following paragraphs we present the measured lake water δ^{2}H and δ^{18}O values, starting with the coastal lakes, followed by the transect lakes.

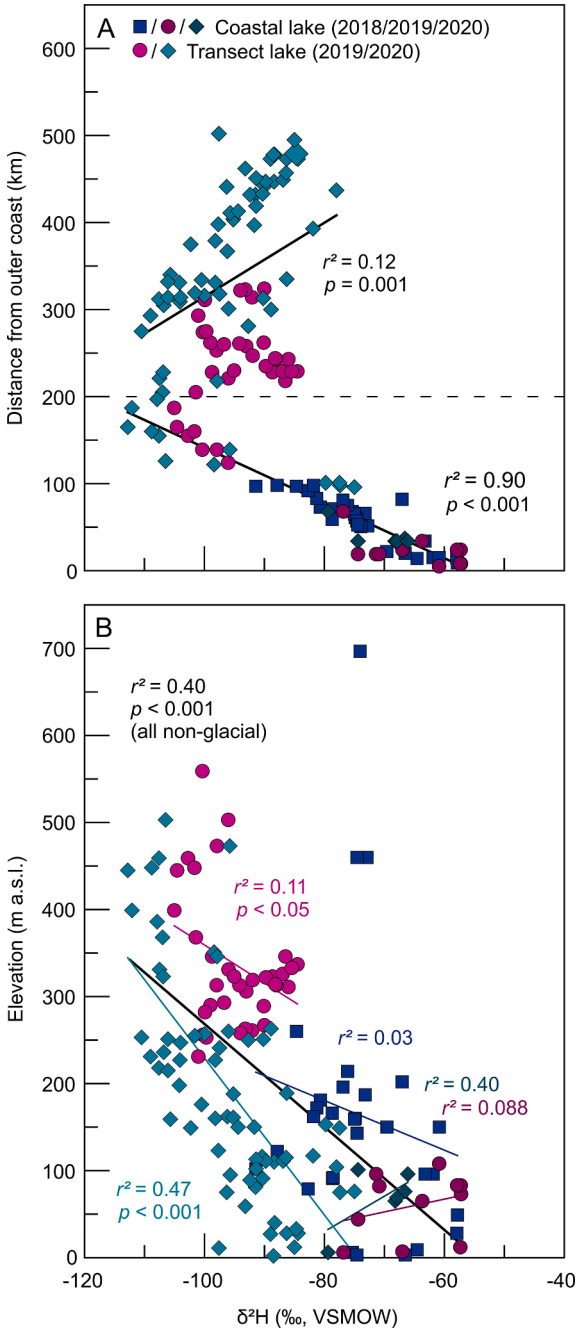

Fig. 5. Spatial trends in lake water δ^{2}H. (a) δ^{2}H versus distance from the outer coast (North Atlantic Ocean or Barents Sea). Linear regression fits are included for all lakes (2018, 2019 and 2020 combined) located less and >200 km from the outer coast (distance = –3.18×δ^{2}H – 176.19 and distance = 4.25×δ^{2}H + 739.39, respectively), separated by dashed line. (b) δ^{2}H versus elevation, with linear regressions for each subset of coastal and transect lakes (2018, 2019 and 2020), as well as for all non-glacial lakes (excluding three high-elevation lakes (>460 m a.s.l.) and one lake close to sea level receiving glacial meltwater).

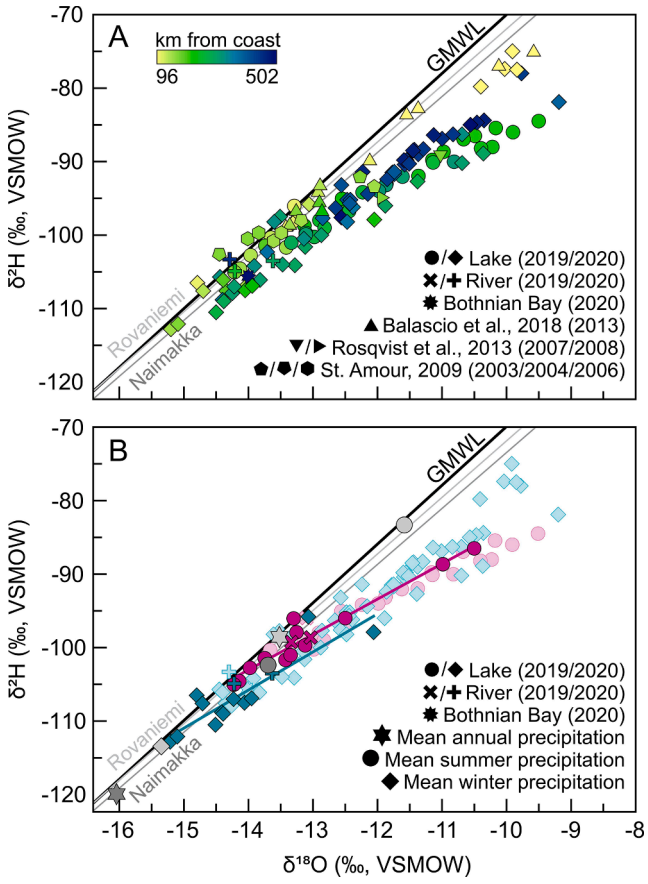

Fig. 6. δ^{18}O versus δ^{2}H values for transect lakes and rivers sampled in 2019 and 2020, colored by distance to the North Atlantic coast (a), and by sampling year (b). (a) includes lakes sampled in the study area by St. Amour (2009) and Balascio et al. (2018), and lake surface water (depth ≤ 1 m) from Guossajavri (Rosqvist et al., 2013; Fig. 1). Dark symbols in (b) show lakes (n = 12) and locations along the Muonio River (n = 2) sampled both year, and light symbols are all samples. Local evaporation lines (LELs) for 2019 (δ^{2}H = 4.82×δ^{18}O – 35.58) and 2020 (δ^{2}H = 5.18×δ^{18}O – 33.27) are included for the 12 resampled lakes. Local meteoric water lines and amount-weighted mean annual and seasonal precipitation values (winter = November-May; summer = June-October) for Naimakka and Rovaniemi are displayed in grey.

All lakes along the outermost coast plot in the upper right corner of the co-isotope plot (Fig. 3). In 2018, δ^{2}H and δ^{18}O of 30 coastal lakes ranged from –91.43 to –57.82‰ (median = –74.72 ± 8.36‰ (±1σ)) and –12.85 to –7.48‰ (median = –10.64 ± 1.23‰), respectively. Deuterium excess ranged from –3.00 to + 14.37‰ (median = 9.10 ± 3.59‰). In 2019, δ^{2}H and δ^{18}O of 11 coastal lakes ranged from –76.84 to –57.22‰ (median = –63.69 ± 7.11‰) and –11.27 to –8.02‰ (median = –9.19 ± 0.88‰), respectively. For these lakes, d-excess ranged from 2.52 to 15.12‰ (median = 9.85 ± 4.20‰). δ^{2}H and δ^{18}O of six coastal lakes sampled in 2020 ranged from –79.40 to –66.10‰ (median = –68.05 ± 4.85‰) and –11.83 to –9.68‰ (median = –10.07 ± 0.78‰), respectively. Deuterium excess ranged from 11.30 to 15.20‰ (median = 12.65 ± 1.49‰). For lakes sampled along the NW-SE transect in 2019 (n = 35), δ^{2}H and δ^{18}O ranged from –105.04 to –84.49‰ (median = –95.05 ± 5.82‰) and –14.22 to –9.50‰ (median = –12.44 ± 1.32‰), respectively (Figs. 3–7). Deuterium excess of these lakes ranged from –8.47 to + 10.28‰ (median = 3.55 ± 4.97‰). For transect lakes sampled in 2020 (n = 68), δ^{2}H and δ^{18}O ranged from –112.80 to –75.00‰ (median = –95.75 ± 9.35‰) and –15.20 to –9.19‰ (median = –12.43 ± 1.51‰), respectively. Deuterium excess ranged from –8.40 to 11.80‰ (median = 3.25 ± 3.84‰). All transect lakes plot along a LEL (δ^{2}H = 5.50×δ^{18}O –

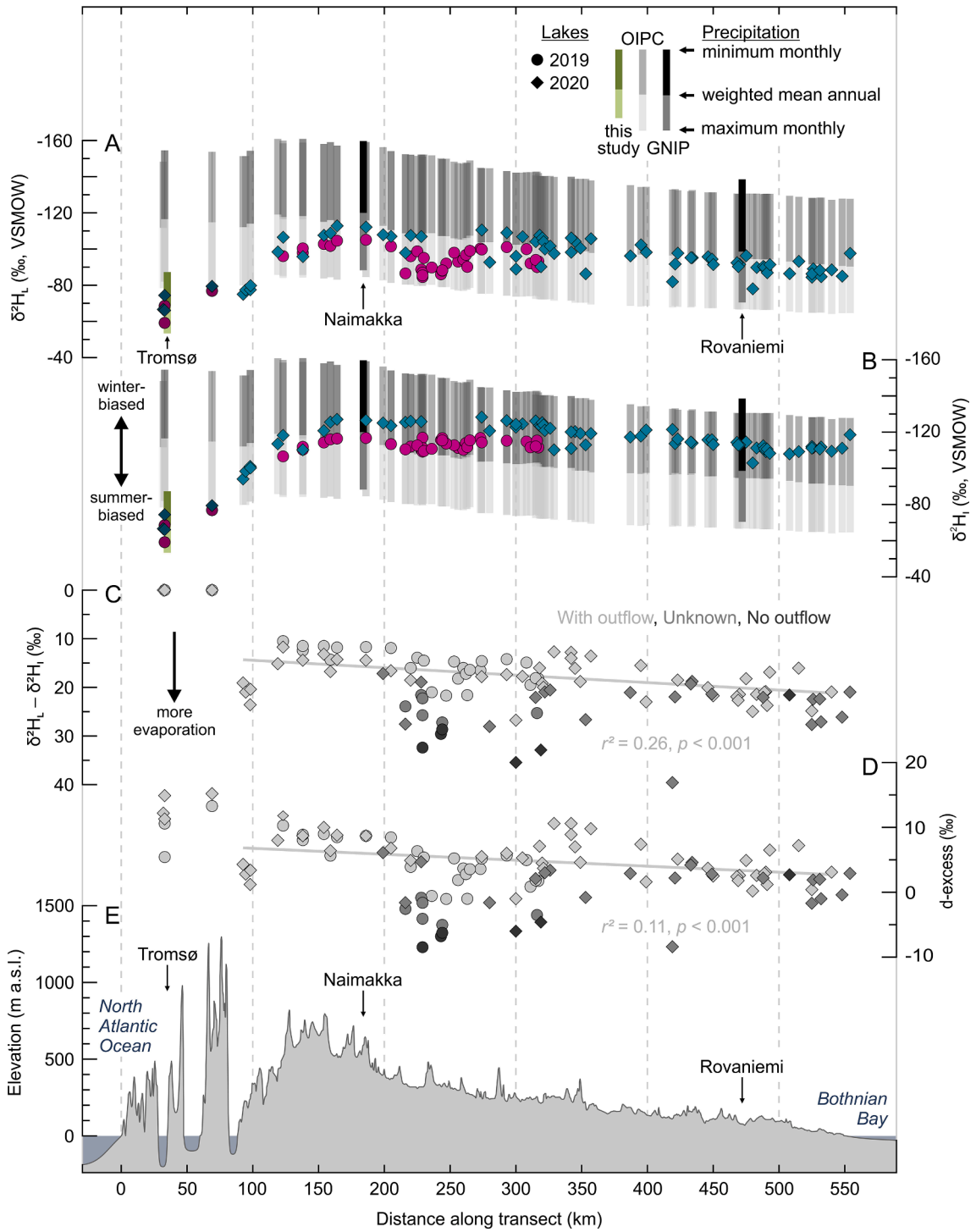

Fig. 7. Lake water δ^2H_L (a), inferred inflow δ^2H_I (b), offset between δ^2H_L and δ^2H_I (c), d-excess (d), and elevation (e) for all lakes along transect (colors and shapes as in Fig. 3). Four coastal lakes along an extension of the transect (NW of Skibotn; Fig. 1) are plotted for comparison. Vertical bars in (a-b) represent the ranges between weighted mean annual and maximum and minimum monthly precipitation δ^2H in Tromsø (this study), Naimakka and Rovaniemi (GNIP; IAEA/WMO, 2019), and for the location of each lake, modeled using the Online Isotopes in Precipitation Calculator (OIPC; Bowen, 2021). Symbols in (c-d) are colored according to throughflow regime (with outflow, without outflow, or unknown), and linear regression fits are included for all through-flowing lakes ($\delta^2H_L - \delta^2H_I = 0.015 \times \text{distance} + 12.89$; d-excess = $-0.0092 \times \text{distance} + 7.69$). Note that the y-axes in (a-c) are inverted.

27.55; Fig. 3), a further indication that some of the lakes undergo evaporation.

Transect lakes sampled in both 2019 and 2020 ($n = 12$) generally showed similar interannual variability (Fig. 6b and 8). Samples collected in 2020 were ^2H-depleted relative to samples collected from the same lakes in 2019 (Fig. 6b and 8) but had similar d-excess both years. The average offset (2020 minus 2019) was –8.43‰ for δ^2H and + 0.90‰ for d-excess. One large lake (Kilpisjärvi; 69.05°N, 20.79°E, 37 km^2) was slightly ^2H-enriched in 2020 compared to 2019, with an offset of + 2.12‰ for δ^2H and + 0.66‰ for d-excess (Fig. 8a). Applying linear regression fits to these 12 lakes resulted in LELs with the equations $\delta^2H = 4.82 \times \delta^{18}O - 35.58$ and $\delta^2H = 5.18 \times \delta^{18}O - 33.27$, for 2019 and 2020

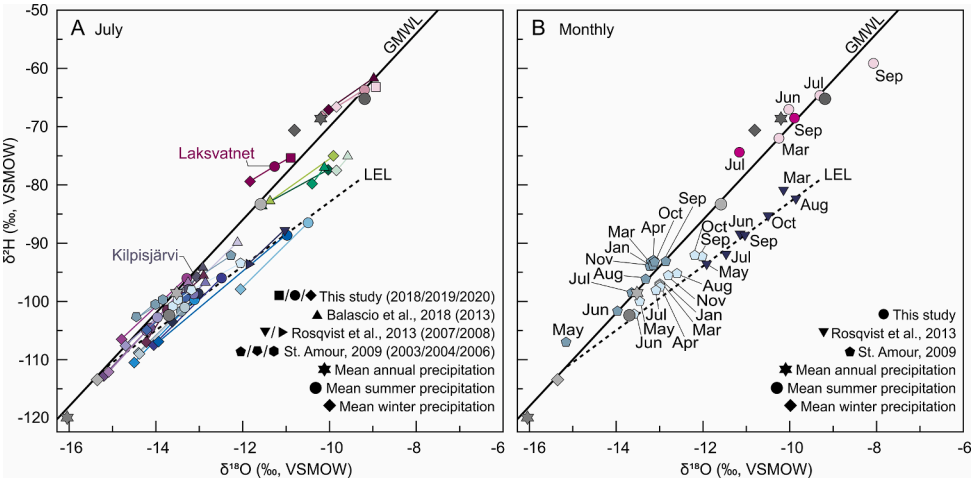

Fig. 8. (a) Interannual variability in summer (July) lake water δ^2H and $\delta^{18}O$ from this study (2018–2020), lakes sampled in the same area (St. Amour, 2009; Balascio et al., 2018) and lake Guossajavri (Rosqvist et al., 2013; 125 km SW of our transect). Lakes water samples collected from the same lakes in July different years (from 2013 to 2020) are illustrated in the same color and connected with lines. Coastal lakes are colored pink, lakes in the Skibotn valley are green, and transect lakes are purple and blue. (b) Monthly average isotopic composition of lakes sampled 1–4 years from 2002 to 2020. All samples were taken at the surface (this study: *c.* 10 cm below the lake surface) from the shoreline, or from in the middle of the lake (depth ≤ 1 m). Samples from inlets were excluded. Amount-weighted mean annual and seasonal precipitation values (winter = November-May; summer = June-October) are displayed in grey (dark grey = Tromsø; middle grey = Naimakka; light grey = Rovaniemi), and black dashed line represents the local evaporation line (LEL; $\delta^2H = 5.50 \times \delta^{18}O - 27.55$) for transect lakes in this study. For locations, see Fig. 1. (For interpretation of the references to color in this figure legend, the reader is referred to the web version of this article.)

respectively (Fig. 6b). Two locations along the Muonio River exhibited similar interannual variation as the lakes (Fig. 6b), indicating different inflow values in 2019 and 2020. In 2019, the river water had δ^2H of –98.62 and –99.24‰, respectively. In 2020, the same two sites along the river had δ^2H of –103.50 and –104.90‰, resulting in an average offset of –5.27‰. The average offset for d-excess was + 0.69‰. One sample collected from the Bothnian Bay in 2020 had δ^2H and $\delta^{18}O$ of –105.60 and –14.00‰, respectively, reflecting the high river-runoff to this northernmost part of the Baltic Sea (Figs. 3, 4 and 6).

The four northernmost lakes in the transect (located in Skibotn; Fig. 1b) had relatively enriched δ^2H and $\delta^{18}O$ values compared to the rest of the transect lakes (Figs. 4, 8 and S1). δ^2H and $\delta^{18}O$ ranged from –79.80 to –75.00‰ (median = –77.45 ± 1.70‰) and from –10.40 to –9.84‰ (median = –9.97 ± 0.22‰), respectively. Deuterium excess ranged from 1.20 to 4.30‰ (median = 3.10 ± 1.13‰). These four lakes are located within 9 km from the Lyngen fjord, and could therefore be considered coastal (Figs. 1 and 4). However, there is a strong rain-shadow effect in Skibotn, where the mean annual precipitation is 465 mm (MET Norway, 2021), compared to 1091 mm in Tromsø, located on the other side of the Lyngen Alps (Fig. 1c), *c.* 60 km northwest of Skibotn.

For lakes by the coast and along the beginning of the transect (<*c.* 200 km from the North Atlantic) there is a significant ($p < 0.001$) trend toward more ^2H-depleted lakes moving away from the coast, whereas farther inland, this trend is still significant ($p = 0.001$), though reversed (Fig. 5a). δ^2H also decreases with elevation (Fig. 5b). This trend is significant for the transect lakes ($p < 0.05$ and $p < 0.001$ in 2019 and 2020, respectively), but not for the coastal lakes. Considering the strong correlation between δ^2H and $\delta^{18}O$ for both coastal ($r^2 = 0.84$) and transect ($r^2 = 0.92$) lake samples, we assume that trends in $\delta^{18}O$ follow δ^2H and hereafter primarily focus on δ^2H and d-excess.

4.2. Inferred inflow δ^2H values

The conventional LEL-MWL intersection approach yielded δ^2H_I values for the transect lakes of –104.78 and –112.90‰ in 2019 and 2020, respectively. Bayesian inflow modeling, which we did for all 91 transect lakes, yielded δ^2H_I ranging from –116.87 to –106.57‰ (median = –112.72 ± 2.57‰) in 2019, and –128.27 to –94.08‰ (median = –115.75 ± 7.53‰) in 2020. This is on average 18.27‰ (2019) and 20.55‰ (2020) more ^2H-depleted than measured lake water δ^2H (Fig. 7). The 90% confidence intervals for δ^2H_I ranged from –148.44 to –111.52‰ for the lower bound and from –118.11 to –83.00‰ for the upper bound, with an average of –132.30 and –104.26‰, respectively. For comparison, δ^2H_L for the coastal lakes ranged from –91.43 to –57.82‰ (median = –74.72 ± 8.36‰) in 2018, –76.84 to –57.22‰ (median = –63.69 ± 7.11‰) in 2019, and from –79.40 to –66.10‰ (median = –68.05 ± 4.85‰) in 2020.

In the area with lakes sampled in both 2019 and 2020 (<320 km from the North Atlantic), δ^2H_I values were ^2H-depleted in 2020 compared to in 2019. For the 12 resampled lakes, δ^2H_I ranged from –116.72 to –106.57‰ (median = –113.79 ± 2.97‰) in 2019, and –128.27 to –110.21‰ (median = –125.67 ± 4.87‰) in 2020, resulting in an average offset of –10.68‰ (Fig. 7). Kilpisjärvi had a similar, but slightly more negative inferred δ^2H_I value in 2019 (–110.30‰) compared to 2020 (–110.21‰), with an offset of + 0.09‰. In 2020, the four lakes in Skibotn had δ^2H_I values from –101.06 to –94.08‰ (median = –99.27 ± 2.69‰), comparable to coastal δ^2H_L, whereas the rest of the transect lakes had δ^2H_I ranging from –128.27 to –102.94‰ (median = –116.72 ± 6.23‰).

Moving inland, δ^2H_I decreased rapidly in the first *c.* 160 km along the transect, after which δ^2H_I stayed relatively stable, with a slightly increasing trend towards the Bothnian Bay. Generally, lakes closer to the North Atlantic had δ^2H_L closer to inferred δ^2H_I, for through-flowing lakes δ^2H_L-δ^2H_I increased moving southeast along the transect (+1.53‰ per 100 km), and closed basins had the largest offsets between δ^2H_L and δ^2H_I (Fig. 7c).

5. Discussion

Lake water isotopes in our study area display mainly two kinds of variability, caused by differences in 1) inflow value (moving along the MWL) and 2) evaporation (moving below the MWL; Fig. 3). In most cases, lake water inflow values reflect a mixture of sources with different isotopic composition (e.g., summer and winter runoff, groundwater). The seasonality of lake water is primarily governed by the lake water residence time, since this determines the proportion of summer and winter precipitation in the lake (Jonsson et al., 2009). The position of a lake along the MWL and its relation to local precipitation isotopic composition can thus give information about lake water biases toward summer or winter season precipitation. In δ^2H-$\delta^{18}O$ space, lakes experiencing evaporative enrichment (decreasing d-excess) plot below the MWL, and along LELs. In the following sections, we discuss the sensitivity of modern lake water δ^2H along the climate gradient to differences

in inflow isotopic composition and evaporation, how these two controls vary in time and space, and why this variability needs to be considered when inferring lake-water-isotope proxy records.

5.1. Regional variability in lake water δ^2H and inferred inflow δ^2H

5.1.1. Coastal lakes

The strong correlation between increasing distance from the coast and decreasing δ^2H_L ($r^2 = 0.90$, $p < 0.001$; Fig. 5a) for the lakes closest to the coast (<*c.* 200 km; both coastal and the northernmost part of the transect), suggests that distillation during atmospheric moisture transport, prior to precipitation, is the most important control on δ^2H_L for coastal lakes in this area. δ^2H and $\delta^{18}O$ decrease by *c.* 57‰ and 6.8‰ over 200 km, or 28‰ and 3.4‰ per 100 km, respectively (Fig. 5a). In the Pacific Northwest, USA (mountainous but drier than coastal Norway), the $\delta^{18}O$ isotopic gradient is 1.2‰ per 100 km (Welker, 2000) and in the Sierra Nevada, USA (wet year-round, most precipitation in winter, some mountains) 5‰ per 100 km (Ingraham & Taylor, 1991). Across the European Plain (from mild and wet coastal Ireland to the continental foothills of the Ural Mountains), the gradient is 0.2‰ per 100 km (Rozanski et al., 1993). This means that our gradient is within ranges found elsewhere and most similar to gradients in similar environments (wet, mountainous, coastal). The least ^2H-depleted lakes are the ones at the northern coast and the outermost coast to the west of Tromsø (Fig. 4), since the transport from the source is shorter and there is not much rain-out prior to precipitation. Three lakes in Kirkenes are slightly ^2H-depleted compared to the other lakes at the outermost coast (Fig. 1b and 4). None of these lakes have distinct outflows, and relatively low d-excess (Supplementary Fig. S1) suggests they are likely experiencing evaporative enrichment. They may also receive source water with a slightly different isotopic signal, being located near the Barents Sea. Lakes near Tromsø are relatively ^2H-enriched compared to lakes slightly farther from the coast (Fig. 4).

In the coastal region, most of the large through-flowing lakes plot close to the MWL, whereas some smaller lakes with low or unknown throughflow and long residence times fall below the MWL, being more affected by evaporation (Fig. 3). A couple of large through-flowing lakes with large mountainous catchments plot above the MWL and close to Tromsø amount-weighted winter precipitation (e.g., Laksvatnet; Fig. 4a and e, 8), suggesting a longer response time, and that the depleted meltwater from snow has not yet been flushed through in early July.

Some of the local variability in coastal lake water δ^2H can also be explained by differences in elevation (Fig. 5b), likely reflecting heterogeneous airflow patterns, with fjords funneling onshore winds and mountains causing orographic precipitation. The mountains cause the air masses to rise as they move inland from Tromsø, causing rainout and more negative δ^2H values (Figs. 4, 5 and 7). Lakes at a given distance from the coast have similar isotope values, despite differences in elevation (Fig. 5a-b). This is likely because precipitation at a given location forms at the same elevation in the atmosphere, and that elevation rises over the mountains moving inland. Three high elevation coastal lakes (>460 m a.s.l.) have δ^2H_L values comparable to other coastal lakes, despite their high elevation (Fig. 5b). They have high d-excess (average = 14.2 ± 0.3‰) and plot above the MWL, suggesting that their isotopic signals are biased toward winter precipitation. In Tromsø, precipitation δ^2H is relatively enriched compared to the more inland stations and does not show a strong seasonality. In contrast, d-excess is significantly higher in fall and winter than in summer (Figs. 2 and 3), due to kinetic fractionation effects when snow forms in mixed-phase clouds (vapor supersaturated over ice; Jouzel & Merlivat, 1984). It is common for mountain lakes to receive most precipitation as snowfall and for their catchments to experience late snowmelt, explaining the high d-excess lake water values. Furthermore, two of the lakes have small niche glaciers in their catchments, contributing glacial meltwater. Thus, our dataset suggests that coastal lakes are primarily influenced by varying degrees of distillation during atmospheric moisture transport, precipitation amount and lake and catchment morphometry, the latter two determining the lake water residence time.

5.1.2. Transect lakes

In contrast to the coastal lakes, most of the transect lakes experience more evaporative enrichment, plotting below the MWL and along a LEL (Figs. 3 and 6). Lake surface water from Oikojärvi (located close to Naimakka; St. Amour, 2009) and Guossajavri (125 km SW of our transect; Rosqvist et al., 2013; Fig. 1b) sampled between 2002 and 2008 fall along similar LELs, suggesting similar evaporation patterns on a regional scale and between years (Figs. 6 and 8). The North Atlantic is still the main moisture source, so precipitation δ^2H, and as a result lake water δ^2H, becomes more and more depleted the first *c.* 160 km along the transect, reflecting Rayleigh distillation during moisture transport (Figs. 4–7).

On the southeastern side of the mountains, where the relief changes from highlands with incised valleys to a gently sloping plain with few hills, there is a larger spread in δ^2H_L (Fig. 7a) and larger and more variable offsets between δ^2H_L and δ^2H_I (Fig. 7c). This coincides with the northern boundary of the northern aapa mire zone, where large, branched mire systems are common (Ruuhijärvi, 1983). Although lakes in wetland-dominated catchments tend to have low E/I (Gibson et al., 2002), many of the lakes in this area are evaporatively enriched, plotting on a LEL and having low d-excess (Figs. 3, 6 and 7d). Hydrologically closed basins, lack of clear surface flow, and/or only seasonal connection by small streams or wetland areas may make these lakes susceptible to evaporation. Furthermore, in continental regions at high latitudes, seasonally arid conditions can increase the evaporative enrichment during the thaw season (Gibson et al., 2005). Smaller inter-lake variation in δ^2H_I than in δ^2H_L (Fig. 7a-c), suggests that most lakes have similar inflow seasonality and sources, whereas evaporation, indicated by decreasing d-excess (–0.92‰ per 100 km; Fig. 7d), increases moving southeast. Moreover, some lakes possibly have δ^2H_L values influenced by factors in addition to evaporative enrichment.

Some of the lakes might be groundwater fed, since till and glaciofluvial aquifers are common in this region (Kortelainen & Karhu, 2004). However, there are no significant differences between the isotopic composition of precipitation and shallow groundwater (till aquifers) in northern Finland and Sweden (Kortelainen & Karhu, 2004). Both follow the same seasonal cycle with most enriched values in late fall, and most depleted values after snowmelt. We do therefore not expect shallow groundwater recharge to the lakes to significantly alter δ^2H_L.

Lakes on the southeastern side of the Scandinavian mountains most likely also receive precipitation from other moisture sources, such as the Baltic region and Eurasia. These sources are more depleted (Schmidt et al., 1999; Bailey et al., 2021), but the travel distance may be shorter, potentially resulting in less distillation and precipitation that is relatively enriched compared to Atlantic moisture, a phenomenon also observed in precipitation events in Arctic Alaska (Putman et al., 2017). In summer, precipitation can be induced by local convection, and less influenced by atmospheric circulation (Jaagus, 2009). Local moisture could in this way at least partly explain the slightly enriched δ^2H_L of lakes closest to the Bothnian Bay (Fig. 7a). Furthermore, transpiration, another process most important in summer, can partly compensate for isotopic depletion caused by distillation during moisture transport, by recycling soil moisture without fractionation (Rozanski et al., 1982). The relative contribution of moisture from different source regions and the resulting isotopic compositions of precipitation can be assessed on an event basis at a given station (Bailey et al., 2021; Mellat et al., 2021), but we do not have any data on this over longer time scales (i.e., covering our study period), or know how it varies within our study region. Most likely, the isotopic composition of precipitation along our transect, and therefore lake water inflow, is controlled by a combination of different moisture source regions, local convection, and evapotranspiration.

5.1.3. Lake location and inflow seasonality

Comparing δ^2H_I to precipitation δ^2H data from Tromsø, Naimakka and Rovaniemi, as well as OIPC-modeled precipitation δ^2H (Bowen, 2021), suggests that winter precipitation is more important for inland lakes, whereas coastal lakes tend to be summer-biased or have an isotopic composition close to mean annual precipitation δ^2H (Fig. 7b). A similar trend is seen on western Greenland, likely reflecting lake water inflow seasonality along an aridity gradient (Cluett & Thomas, 2020). In our study area, the inland region normally receives a greater fraction of the annual precipitation during the summer months (Fig. 2). This lake water bias towards winter precipitation for inland lakes is likely due to lower relative humidity and higher evapotranspiration at inland sites in

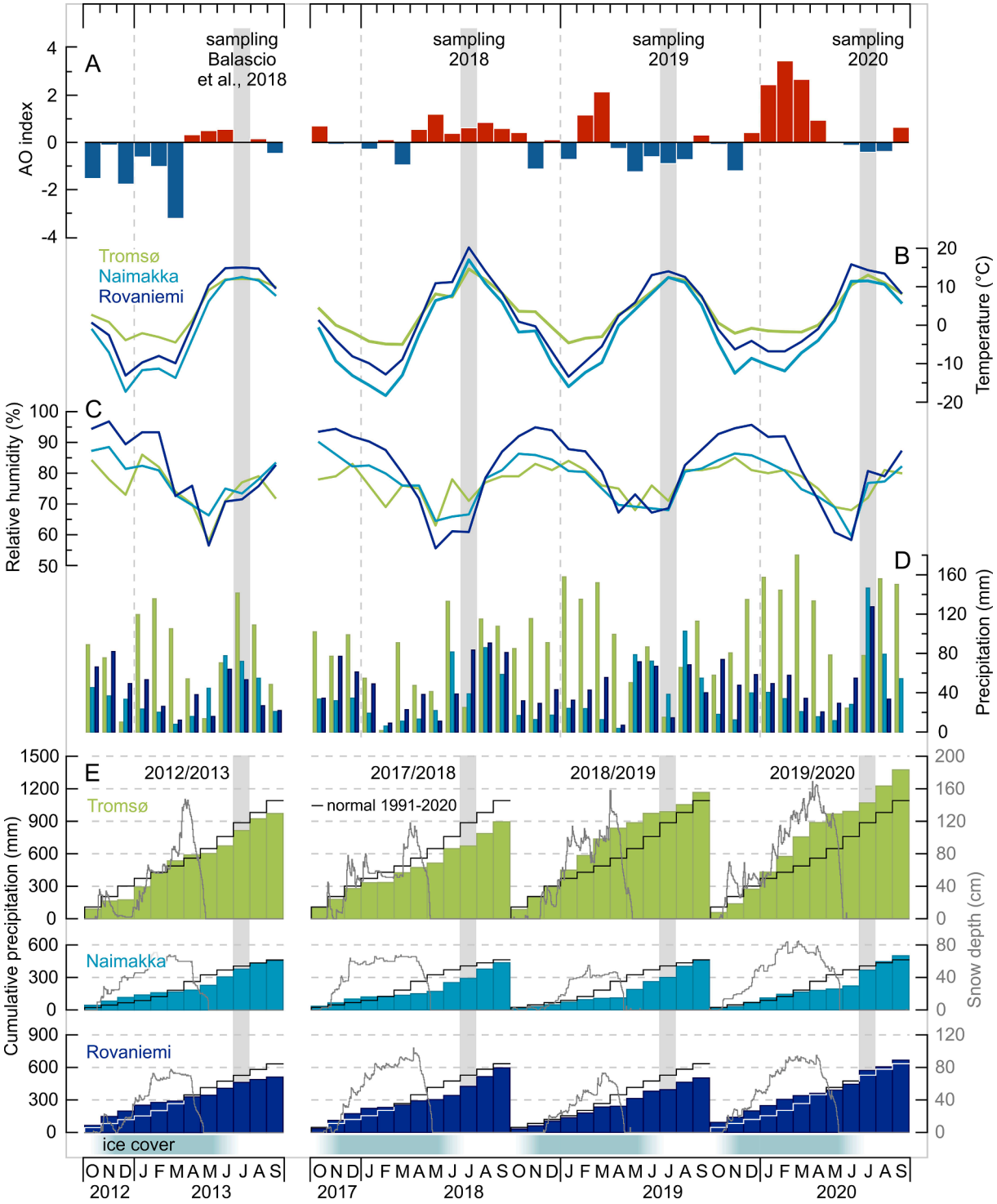

Fig. 9. (a) Monthly Arctic Oscillation (AO) index (National Weather Service Climate Prediction Center, 2021). (b) Mean monthly air temperature, (c) relative humidity, (d) accumulated precipitation and (e) cumulative precipitation and snow depths for the hydrological years (October-September) 2012/2013, 2017/2018, 2018/2019 and 2019/2020 for Tromsø, Naimakka and Rovaniemi (FMI, 2021; MET Norway, 2021; SMHI, 2021). Black stepped lines in (e) illustrate mean cumulative precipitation values for 1991–2020. Snow depths for Naimakka were obtained from Saarikoski (68.81°N, 21.25°E, 450 m a.s.l.), 18 km NW of Naimakka (SMHI, 2021).

summer (Fig. 2), even if a greater fraction of total precipitation falls in summer (Bowen et al., 2018).

That coastal lakes appear to be summer-biased is somewhat unexpected, considering that Tromsø receives more winter precipitation than Naimakka and Rovaniemi (Figs. 2 and 9d-e). OIPC-modeled precipitation δ^2H values are based on interpolation using GNIP values. They are therefore biased towards the nearest GNIP stations (i.e., Naimakka and Rovaniemi), which are more continental and experience a larger seasonality than Tromsø (Figs. 2 and 3). We compare the OIPC values with precipitation samples collected in Tromsø in 2019–2021 and can confirm that the modeled coastal values are, indeed, too depleted compared to our new precipitation isotope dataset (Fig. 7a-b). However, it cannot be excluded that the ^2H-depleted winter isotopes might have been efficiently flushed from some coastal lakes with short residence times, especially considering the high precipitation amounts in June 2018 and 2019 (Fig. 9). This suggests that lakes in this region likely reflect a range of summer to mean annual to winter-biased precipitation δ^2H (Figs. 3 and 7).

5.2. Lake water δ^2H and inferred inflow δ^2H changes over time

5.2.1. Interannual variability

Sampling campaigns concentrated in the first week of July in 2018, 2019 and 2020 allowed us to get an insight into the interannual variability in δ^2H_L and δ^2H_I. We focus this comparison on the transect lakes, since we sampled coastal lakes in different locations each year (i.e., in the Tromsø area vs. along the northern coast). Only three coastal lakes were sampled two or three of these years, and they follow similar interannual patterns as the transect lakes (Fig. 8a). We sampled the transect lakes in 2019 and 2020, and extended the transect farther southeast in 2020 (Fig. 7). Twelve transect lakes sampled in both years had more ^2H-depleted δ^2H_L in 2020, and a LEL intersecting the MWL at a more depleted value compared to 2019 (Fig. 6b and 7a), suggesting more depleted inflow water in 2020 than in 2019. This is supported by more depleted modeled δ^2H_I in 2020 compared to in 2019 (Fig. 7b). We suggest that the more ^2H-depleted values in 2020 were a response to 1) more precipitation in winter 2019/2020 than in 2018/2019 (Fig. 9d–e), 2) later spring melt in 2020 than 2019 (Fig. 9e) resulting in less time prior to our July sampling for ^2H-enriched summer precipitation to flush the ^2H-depleted winter melt out of the lakes, and/or 3) more May-June rainfall in 2019 than in 2020 (Fig. 9d) contributing to higher snowmelt bypass in 2019 (i.e., more snow melting off the high-elevation portions landscape before the lakes become ice free in the first half of June), which would remove ^2H-depleted winter precipitation from the catchment without entering the lake. The high precipitation amounts in January-March 2020 were associated with extreme AO+ conditions and an exceptionally strong stratospheric polar vortex, causing strong winter westerlies that carried greater-than-average amounts of moisture from the North Atlantic over Fennoscandia (Lawrence et al., 2020; Fig. 9a, d-e).

An additional explanation for ^2H-depleted lake inflow values in 2020 could be a change in moisture source. Surface waters in the Baltic Sea are relatively ^{18}O-depleted compared to the North Atlantic (Schmidt et al., 1999), and a greater influence of Baltic moisture to our study area could therefore contribute to more depleted precipitation. In winter 2018/2019 most of the Bothnian Bay was sea-ice covered, whereas winter 2019/2020 Baltic Sea sea-ice cover set a record for minimum winter extent in the 120-year-long measuring period (Sjöfartsverket & SMHI, 2020a, 2020b). However, predominantly southwesterly winds and pressure systems moving eastward over the Baltic Sea in both years imply a low impact of Baltic Sea moisture to our study area during this period.

Some lakes in the area have been sampled in previous studies, allowing us to extend our interannual comparison further back in time. In 2013, nine of the transect lakes were relatively enriched compared to the same lakes sampled in 2019 and/or 2020 (Balascio et al., 2018; Fig. 6a and 8). The interannual changes in lake water isotopic composition were parallel to the MWL, suggesting that the lakes had more ^2H-enriched inflow water in 2013 than in 2019 and 2020, but that all years had a similar influence of evaporation. The hydrological year 2012/2013 was relatively dry compared to 2018/2019 and 2019/2020 (especially in Tromsø; Fig. 9d-e). However, June and July 2013 were wet (Fig. 9d), and the lakes were sampled several weeks later than in 2019 and 2020 (July 26, 2013; N. Balascio, personal communication), suggesting that the relatively enriched lake water values reflect greater summer precipitation inflow to the lakes in 2013. Two lakes close to Naimakka (Oikojärvi and Keitjoru) that were sampled by St. Amour (2009) in July 2003, 2004 and 2006 displayed a similar magnitude of interannual variability to the lakes in our dataset (Fig. 8a). The Oikojärvi samples from July 2004 and 2006 were close to the MWL, whereas the 2003 sample was evaporatively enriched along a LEL, perhaps due to exceptional dryness that year, as suggested by St. Amour (2009).

5.2.2. Seasonal variability

The lake water isotopic composition also follows a seasonal cycle. St. Amour (2009) collected monthly samples (excluding February and December) from the two lakes in Naimakka from 2002 to 2005, generally recording lowest values in the beginning of the ice-free season due to isotopically depleted snowmelt, increasing values over summer due to more enriched inflow isotopic composition and/or evaporative enrichment, and high and relatively stable composition during the ice-cover season (Fig. 8b). Guossajavri, northern Sweden, showed a similar trend in 2007 and 2008, with the lake moving up along the LEL during the summer months, and being recharged in winter (Rosqvist et al., 2013; Fig. 8b). This is in agreement with other lakes in northern Sweden (Jonsson et al., 2009) and elsewhere in the Arctic (Leng & Anderson, 2003; Tondu et al., 2013).

We sampled two lakes in Tromsø in March, June, July and/or September in 2018–2020. Except for a low March value, the seasonal isotope patterns in these lakes are similar to interannual patterns in all the lakes: isotope values tend to move parallel to the MWL, implying changes in inflow isotopic composition, rather than changes in evaporation. Although we do not have samples to examine seasonal variability in the transect lakes, given the similarities in interannual variability between the coast and transect, we hypothesize the transect lakes experience similar seasonal changes in inflow isotopic composition, with constant influence of evaporative enrichment.

5.3. Implications for precipitation proxy reconstructions

Interpreting isotope proxy records often assumes that, for a given record, the control on the lake water isotopic variability is constant through time. We have demonstrated that lakes in this region display variable sensitivity to changes in inflow (precipitation) isotopic composition and to evaporative enrichment, and that these controls vary in both time and space. Resolving these controls on modern lake water isotopes is important for making quantitative paleoclimate inferences. Depending on what aspect of the hydrological cycle we aim to reconstruct (e.g., atmospheric circulation, precipitation amount or seasonality, moisture balance), we can target different lakes.

In parts of our study area, modern precipitation isotopes have strong seasonal variability (Figs. 2 and 7), and if this signal is preserved in lake sediment proxy records, we can use it to reconstruct changes in precipitation seasonality (Cluett & Thomas, 2020; Thomas et al., 2020). The seasonality preserved in a proxy record depends on the δ^2H or $\delta^{18}O$ of source (lake or soil) water at the time of proxy synthesis, which can vary between proxies (Corcoran et al., 2021). Lake water isotopic composition and seasonal variability depends on the lake water residence time (Jonsson et al., 2010; Tondu et al., 2013; Ala-Aho et al., 2018), which may also change through time.

Previous paleoclimate work in northern Fennoscandia suggests that changes in Holocene precipitation isotopes are strongly linked to

changes in air temperature and air mass sources. Lacustrine carbonates, biogenic silica, and cellulose from non-evaporated lakes in northern Sweden have been used to reconstruct past changes in lake water $\delta^{18}O$ and precipitation (Shemesh et al., 2001; Hammarlund et al., 2002; Rosqvist et al., 2004, 2007, 2013; St. Amour, 2009; Jonsson et al., 2010). In most of these studies, depleted summer lake water $\delta^{18}O$ was inferred to reflect increased influence of Arctic air masses. Furthermore, Rosqvist et al. (2013) suggested that periods of relatively high $\delta^{18}O_{diatom}$ reflect a dominance of summer precipitation, related to a positive AO index, whereas low $\delta^{18}O_{diatom}$ reflects dominant winter precipitation due to positive NAO.

Studying modern conditions can aid proxy interpretations since it allows us to directly link isotopic changes to observations of atmospheric circulation change. Arctic Ocean and Baltic Sea surface waters are relatively depleted compared to North Atlantic moisture (LeGrande & Schmidt, 2006; Bonne et al., 2019), suggesting that depleted precipitation isotopes, and thereby lake water isotopes, may reflect a change to dominance of Arctic or Baltic air masses. However, this will depend on the location of the lake and the moisture travel distance. Atlantic moisture (which is originally less depleted) that has been transported a long distance may have experienced more distillation than more locally derived moisture with a more depleted starting isotopic composition, and therefore also be relatively depleted (Putman et al., 2017; Cluett et al., 2021). Our ^{2}H-depleted lake water values in 2020 were likely not caused by a shift in moisture source region, but by high winter precipitation amounts associated with AO+ conditions and an increase in North Atlantic moisture (Lawrence et al. 2020). Greater-than-average winter precipitation amounts over Fennoscandia can result from both extremely positive and negative winter AO conditions, although from different moisture sources (North Atlantic vs. Barents Sea; Lawrence et al., 2020; Bailey et al., 2021). Complicating things further, modern moisture from the Barents Sea has an isotopic composition comparable to North Atlantic moisture, due to increased strength of the North Atlantic Current (Bailey et al., 2021). If conditions were similar in the past, the Atlantic and Barents Sea moisture sources would be difficult to distinguish from one another in proxy records. Our lake water isotope observations imply that seasonal changes in precipitation amounts need to be taken into account when inferring atmospheric circulation from a proxy record in this region, and that changes in precipitation isotope values can be a result of a change in precipitation seasonality, moisture source, or a combination of both.

For reconstructions of atmospheric circulation and precipitation, we should target lakes that are minimally impacted by evaporative enrichment, since evaporation overprints the precipitation signal. In our dataset, most lakes >100 km from the coast have low d-excess values, suggesting that evaporative enrichment affects them to some degree, regardless of their throughflow regime (Figs. 3, 6a and 7). All transect lakes appear to fall on similar LELs, but with slope and intercept varying from year to year, depending on seasonality (Fig. 6). On interannual and seasonal timescales, changes in inflow appear to have a larger impact than evaporation, with isotope values moving along the MWL (Fig. 8). On longer timescales, evaporation may be more important, making it difficult to disentangle how much of the variability derives from each process (i.e., inflow vs. evaporation). Hence, we suggest that through-flowing coastal lakes are better targets for precipitation reconstructions, since changes in their lake water isotopic composition are more likely to primarily reflect changes in the inflow.

For evapo-concentrated lakes there are a few possible approaches to separate the precipitation from the evaporation signal, including 1) comparing two lakes with contrasting residence times (Anderson et al., 2001), 2) comparing terrestrial and aquatic leaf waxes in the same lake (Rach et al., 2017), or 3) measuring both $\delta^{2}H$ and $\delta^{18}O$ in the same records (Gibson et al., 2005). For the first approach, one needs to identify a non-evaporated lake with short residence time (low $\delta^{2}H_L$-$\delta^{2}H_I$) and one evaporated lake with longer residence time (high $\delta^{2}H_L$-$\delta^{2}H_I$; Anderson et al., 2001). Moreover, the lakes must receive source water reflecting the same precipitation seasonality, and evaporation should be the only factor that differs between the two. The offset between $\delta^{2}H_L$ and $\delta^{2}H_I$ for our transect lakes is >10‰ independent of throughflow, suggesting that it will be difficult to identify an unevaporated lake in this region, which would be needed for this approach. Using the second approach, one compares terrestrial and aquatic leaf wax $\delta^{2}H$ in the same record, which have source water representing the same seasonality. In areas where terrestrial plant source water is evaporatively enriched, but the aquatic plant source water is not, the isotopic difference between the two reflects leaf water evaporative enrichment (Rach et al., 2017; Thomas et al., 2018; Curtin et al., 2019). In contrast, lake water in arid areas has been suggested to be more evaporatively enriched than terrestrial leaf water, meaning that the difference primarily reflects the evaporative enrichment of lake water (Mügler et al., 2008; Balascio et al., 2013). Along our transect, both aquatic and terrestrial leaf waxes likely incorporate a signal of evaporative ^{2}H-enrichment due to low relative humidity and warm conditions in summer (Figs. 2 and 9b-c). Thus, a dual leaf wax approach to separate precipitation and evaporation signals might not be applicable along the transect but may be possible at coastal lakes. For the third approach, one measures $\delta^{2}H$ and $\delta^{18}O$ in the same lakes, which may allow estimation of past changes in the slope of the LEL (Gibson et al., 2005) that could subsequently be used to infer past inflow values. Theoretically, this is possible, however, it involves many uncertainties. First, one needs to analyze the same proxies at the same time slice in several lakes. Second, those two proxies (one with $\delta^{2}H$ and one with $\delta^{18}O$) need to reflect the same pool of water for the same window of time in a season. Moreover, one needs to have good constraints on biosynthetic and other fractionation factors (Brandriss et al., 1998; Sachse et al., 2012; Lombino et al., 2021) to be able to estimate lake water $\delta^{2}H$ and $\delta^{18}O$ and directly compare $\delta^{2}H$ and $\delta^{18}O$ from different proxies (Corcoran et al., 2021).

A more recent approach to guide paleoclimate interpretations is to use proxy system modeling, which uses modern climate variables as inputs to mathematical descriptions of lake water isotope and energy balance (e.g., PRYSM2.0; Dee et al., 2018). By conducting sensitivity tests in which we iteratively change values of one or more climate parameters (e.g., lower relative humidity, more winter precipitation), we can quantify the parameter, or combination of parameters, that could explain changes recorded in lake water isotope proxies. For lakes in our transect, we could for example focus on variables that affect the lake water inflow isotopic signal and amount of evaporative enrichment, to assess the sensitivity of the lake water isotopic composition to these variables. If we have an estimate of how a change in moisture source would affect the precipitation isotopes, we can modify the inflow isotope value in the model to see how this would impact the lake water isotope value. One way to simulate how a shift in moisture source would influence the lake water inflow value is to use a one-dimensional Rayleigh-type distillation model along a theoretical trajectory (Sodemann et al., 2008; Steen-Larsen et al., 2011; Cluett et al., 2021). These approaches can provide us with quantitative constraints on past climate changes.

When interpreting lake-water-derived isotope proxy data from northern Fennoscandia, we need to consider the magnitude of variability in both inflow isotopic composition and evaporation. On the coast, inflow causes more variability than evaporation. Considering the variability among the transect lakes, the ranges for $\delta^{2}H_I$ and $\delta^{2}H_L$ are similar, suggesting that inflow and evaporation might be equally important. Interannual variability is largely due to changes in inflow isotopic composition, however, suggesting the importance of inflow isotopic composition even in lakes that are strongly influenced by evaporation. Therefore, we recommend targeting through-flowing lakes by the coast for precipitation reconstructions. If working with more continental records, we need to address the significance of both inflow and evaporation processes. Importantly, our data show that we cannot interpret all isotopic variability in evapo-concentrated basins in terms of evaporation, as there might also be a substantial variability in inflow isotopic composition through time.

Data availability

Water isotope data are freely available in the Water Isotopes Database at www.waterisotopes.org (Project IDs 00292 (surface waters) and 00293 (precipitation)), and in the Supplementary Information.

CRediT authorship contribution statement

Sofia E. Kjellman: Conceptualization, Investigation, Visualization, Writing – original draft, Project administration, Funding acquisition. **Elizabeth K. Thomas:** Conceptualization, Investigation, Writing – review & editing, Supervision, Funding acquisition. **Anders Schomacker:** Conceptualization, Investigation, Writing – review & editing, Supervision, Funding acquisition.

Declaration of Competing Interest

The authors declare that they have no known competing financial interests or personal relationships that could have appeared to influence the work reported in this paper.

Acknowledgements

This research was supported by grants from the Nansen Foundation and Olle Engkvists Stiftelse (204-0129) to SEK and AS, and NSF grant EAR-IF 1652274 to EKT. We thank Lis Allaart, Jack Percival, and Paul Eric Aspholm for assistance with lake water sampling, and John Arne Opheim, Emma Bender, Marie Bulínová, Carmen Braun, Amicia Lee, and Maxine King for assistance with precipitation collection. We would also like to thank Owen Cowling and Kayla Hollister for instrumental analysis of lake water samples at the Organic and Stable Isotope Biogeochemistry Laboratory at the University at Buffalo, USA. Handling and processing of liquid stable isotope samples was also done at the Norwegian National Infrastructure project FARLAB (Facility for advanced isotopic research and monitoring of weather, climate, and biogeochemical cycling, Project Nr. 245907) at the University of Bergen, Norway. We thank four anonymous reviewers for constructive comments that improved the manuscript.

Appendix A. Supplementary data

Supplementary data to this article can be found online at https://doi.org/10.1016/j.jhydrol.2022.127556.

References

Ala-Aho, P., Soulsby, C., Pokrovsky, O., Kirpotin, S., Karlsson, J., Serikova, S., Vorobyev, S., Manasypov, R., Loiko, S., Tetzlaff, D., 2018. Using stable isotopes to assess surface water source dynamics and hydrological connectivity in a high-latitude wetland and permafrost influenced landscape. J. Hydrol. 556, 279–293. https://doi.org/10.1016/j.jhydrol.2017.11.024.

Alexandersson, H., 2002. *Temperature and precipitation in Sweden 1860–2001*. Swedish Meteorological and Hydrological Institute (SMHI) Meteorological Report No. 104. 28 pp.

Anderson, L., Abbott, M.B., Finney, B.P., 2001. Holocene climate inferred from oxygen isotope ratios in lake sediments, central Brooks Range, Alaska. Q. Res. 55 (3), 313–321. https://doi.org/10.1006/qres.2001.2219.

Bailey, H., Hubbard, A., Klein, E.S., Mustonen, K.-R., Akers, P.D., Marttila, H., Welker, J. M., 2021. Arctic sea-ice loss fuels extreme European snowfall. Nat. Geosci. 14 (5), 283–288. https://doi.org/10.1038/s41561-021-00719-y.

Balascio, N.L., Anderson, R.S., D'Andrea, W.J., Wickler, S., D'Andrea, R.M., Bakke, J., 2020. Vegetation changes and plant wax biomarkers from an ombrotrophic bog define hydroclimate trends and human-environment interactions during the Holocene in northern Norway. Holocene 30 (12), 1849–1865. https://doi.org/10.1177/0959683620950456.

Balascio, N.L., D'Andrea, W.J., Anderson, R.S., Wickler, S., 2018. Influence of vegetation type on *n*-alkane composition and hydrogen isotope values from a high latitude ombrotrophic bog. Org. Geochem. 121, 48–57. https://doi.org/10.1016/j.orggeochem.2018.03.008.

Balascio, N.L., D'Andrea, W.J., Bradley, R.S., Perren, B.B., 2013. Biogeochemical evidence for hydrologic changes during the Holocene in a lake sediment record from southeast Greenland. Holocene 23 (10), 1428–1439. https://doi.org/10.1177/0959683613493938.

Belt, S.T., Cabedo-Sanz, P., Smik, L., Navarro-Rodriguez, A., Berben, S.M., Knies, J., Husum, K., 2015. Identification of paleo Arctic winter sea ice limits and the marginal ice zone: optimised biomarker-based reconstructions of late Quaternary Arctic sea ice. Earth Planet. Sci. Lett. 431, 127–139. https://doi.org/10.1016/j.epsl.2015.09.020.

Bintanja, R., Selten, F.M., 2014. Future increases in Arctic precipitation linked to local evaporation and sea-ice retreat. Nature 509 (7501), 479–482. https://doi.org/10.1038/nature13259.

Bintanja, R., van der Wiel, K., van der Linden, E., Reusen, J., Bogerd, L., Krikken, F., Selten, F., 2020. Strong future increases in Arctic precipitation variability linked to poleward moisture transport. Sci. Adv. 6 (7), eaax6869. https://doi.org/10.1126/sciadv.aax6869.

Blenckner, T., Järvinen, M., Weyhenmeyer, G., 2004. Atmospheric circulation and its impact on ice phenology in Scandinavia. Boreal Environ. Res. 9, 371–380. http://www.borenv.net/BER/pdfs/ber9/ber9-371.pdf.

Bonne, J.-L., Behrens, M., Meyer, H., Kipfstuhl, S., Rabe, B., Schönicke, L., Steen-Larsen, H.C., Werner, M., 2019. Resolving the controls of water vapour isotopes in the Atlantic sector. Nat. Commun. 10 (1), 1–10. https://doi.org/10.1038/s41467-019-09242-6.

Botter, G., Bertuzzo, E., Rinaldo, A., 2010. Transport in the hydrologic response: Travel time distributions, soil moisture dynamics, and the old water paradox. Water Resour. Res. 46 (3) https://doi.org/10.1029/2009WR008371.

Bowen, G. J., 2021. OIPC: The online isotopes in precipitation calculator, version 3.1. Available at: http://www.waterisotopes.org.

Bowen, G.J., Putman, A., Brooks, J.R., Bowling, D.R., Oerter, E.J., Good, S.P., 2018. Inferring the source of evaporated waters using stable H and O isotopes. Oecologia 187 (4), 1025–1039. https://doi.org/10.1007/s00442-018-4192-5.

Brandriss, M.E., O'Neil, J.R., Edlund, M.B., Stoermer, E.F., 1998. Oxygen isotope fractionation between diatomaceous silica and water. Geochim. Cosmochim. Acta 62 (7), 1119–1125. https://doi.org/10.1016/S0016-7037(98)00054-4.

Bring, A., Fedorova, I., Dibike, Y., Hinzman, L., Mård, J., Mernild, S.H., Prowse, T., Semenova, O., Stuefer, S.L., Woo, M.-K., 2016. Arctic terrestrial hydrology: A synthesis of processes, regional effects, and research challenges. J. Geophys. Res. Biogeosci. 121 (3), 621–649. https://doi.org/10.1002/jgrg.v121.310.1002/2015JG003131.

Brosius, L.S., Anthony, K.M.W., Treat, C.C., Lenz, J., Jones, M.C., Bret-Harte, M.S., Grosse, G., 2021. Spatiotemporal patterns of northern lake formation since the Last Glacial Maximum. Quat. Sci. Rev. 253, 106773. https://doi.org/10.1016/j.quascirev.2020.106773.

Clark, I.D., Fritz, P., 1997. Environmental isotopes in hydrogeology. CRC Press, Cambridge, p. 342.

Cluett, A.A., Thomas, E.K., 2020. Resolving combined influences of inflow and evaporation on western Greenland lake water isotopes to inform paleoclimate inferences. J. Paleolimnol. 63 (4), 251–268. https://doi.org/10.1007/s10933-020-00114-4.

Cluett, A.A., Thomas, E.K., Evans, S.M., Keys, P.W., 2021. Seasonal Variations in Moisture Origin Explain Spatial Contrast in Precipitation Isotope Seasonality on Coastal Western Greenland. J. Geophys. Res.: Atmos. 126, e2020JD033543 https://doi.org/10.1029/2020JD033543.

Collins, M., Knutti, R., Arblaster, J., Dufresne, J.-L., Fichefet, T., Friedlingstein, P., Gao, X., Gutowski, W.J., Johns, T., Krinner, G., Shongwe, M., Tebaldi, C., Weaver, A.J., Wehner, M., 2013. Long-term climate change: projections, commitments and irreversibility. In: Stocker, T.F., Qin, D., Plattner, G.-K., Tignor, M., Allen, S.K., Boschung, J., Nauels, A., Xia, Y., Bex, V., Midgley, P.M. (Eds.), *Climate Change 2013: the Physical Science Basis. Contribution of Working Group I to the Fifth Assessment Report of the Intergovernmental Panel on Climate Change*. Cambridge University Press, Cambridge, United Kingdom and New York, NY, USA.

Corcoran, M.C., Thomas, E.K., Morrill, C., 2021. Using a paired chironomid $\delta^{18}O$ and aquatic leaf wax $\delta^{2}H$ approach to reconstruct seasonality on western Greenland during the Holocene. Paleoceanogr. Paleoclimatol. 36 (4), e2020PA004169 https://doi.org/10.1029/2020PA004169.

Craig, H., 1961. Isotopic variations in meteoric waters. Science 133 (3465), 1702–1703. https://doi.org/10.1126/science.133.3465.1702.

Craig, H., & Gordon, L. I. (1965). Deuterium and oxygen 18 variations in the ocean and the marine atmosphere. In: Tongiorgi, E. (Ed.), *Stable Isotopes in Oceanographic Studies and Paleo-Temperatures*. Consiglio nazionale delle ricerche, Pisa, Italy, Spoleto: Conferences in Nuclear Geology. pp. 9-130.

Curtin, L., D'Andrea, W.J., Balascio, N., Pugsley, G., de Wet, G., Bradley, R., 2019. Holocene and Last Interglacial climate of the Faroe Islands from sedimentary plant wax hydrogen and carbon isotopes. Quat. Sci. Rev. 223, 105930. https://doi.org/10.1016/j.quascirev.2019.105930.

Dansgaard, W., 1964. Stable isotopes in precipitation. Tellus 16 (4), 436–468. https://doi.org/10.3402/tellusa.v16i4.8993.

Dee, S.G., Russell, J.M., Morrill, C., Chen, Z., Neary, A., 2018. PRYSM v2. 0: A proxy system model for lacustrine archives. Paleoceanogr. Paleoclimatol. 33 (11), 1250–1269. https://doi.org/10.1029/2018PA003413.

Eklund, A., 1999. *Islägging och islossning på sjöar*. Swedish Meteorological and Hydrological Institute (SMHI) Hydrological Report No. 81. 24 pp.

FMI, 2021. Download observations. Finnish Meteorological Institute, Available at: https://en.ilmatieteenlaitos.fi/download-observations.

Gat, J.R., 1996. Oxygen and hydrogen isotopes in the hydrologic cycle. Annu. Rev. Earth Planet. Sci. 24 (1), 225–262. https://doi.org/10.1146/earth.1996.24.issue-110.1146/annurev.earth.24.1.225.

Gibson, J.J., Birks, S.J., Edwards, T.W.D., 2008. Global prediction of δA and δ^2H-$\delta^{18}O$ evaporation slopes for lakes and soil water accounting for seasonality. Global Biogeochem. Cycles 22, GB2031. https://doi.org/10.1029/2007GB002997.

Gibson, J.J., Edwards, T.W.D., 2002. Regional water balance trends and evaporation-transpiration partitioning from a stable isotope survey of lakes in northern Canada. Global Biogeochem. Cycles 16 (2), 10-1–10-14. https://doi.org/10.1029/2001GB001839.

Gibson, J.J., Edwards, T.W.D., Birks, S.J., St Amour, N.A., Buhay, W.M., McEachern, P., Wolfe, B.B., Peters, D.L., 2005. Progress in isotope tracer hydrology in Canada. Hydrol. Processes: Int. J. 19 (1), 303–327. https://doi.org/10.1002/(ISSN)1099-108510.1002/hyp.v19:110.1002/hyp.5766.

Gibson, J., Prepas, E., McEachern, P., 2002. Quantitative comparison of lake throughflow, residency, and catchment runoff using stable isotopes: modelling and results from a regional survey of Boreal lakes. J. Hydrol. 262 (1–4), 128–144. https://doi.org/10.1016/S0022-1694(02)00022-7.

Gröning, M., 2018. SICalib User Manual (Stable Isotope Calibration for routine δ-scale measurements) Ver 2.16 j. Terrestrial Environment Laboratory (TEL) Technical Note No. 01. International Atomic Energy Agency, Vienna, Austria. 37 pp.

Gröning, M., 2011. Improved water δ^2H and $\delta^{18}O$ calibration and calculation of measurement uncertainty using a simple software tool. Rapid Commun. Mass Spectrom. 25 (19), 2711–2720. https://doi.org/10.1002/rcm.5074.

GTK, 2021. Surficial Deposits of Finland 1:1 000 000. Geological Survey of Finland. Available at: https://gtkdata.gtk.fi/Maankamara/index.html.

Hammarlund, D., Barnekow, L., Birks, H.J.B., Buchardt, B., Edwards, T.W., 2002. Holocene changes in atmospheric circulation recorded in the oxygen-isotope stratigraphy of lacustrine carbonates from northern Sweden. The Holocene 12 (3), 339–351. https://doi.org/10.1191/0959683602hl548rp.

Heidbüchel, I., Troch, P.A., Lyon, S.W., Weiler, M., 2012. The master transit time distribution of variable flow systems. Water Resour. Res. 48 (6), 1–19. https://doi.org/10.1029/2011WR011293.

Hirvas, H., Lagerbäck, R., Mäkinen, K., Nenonen, K., Olsen, L., Rodhe, L., Thoresen, M., 1988. The Nordkalott Project: studies of Quaternary geology in northern Fennoscandia. Boreas 17 (4), 431–437. https://doi.org/10.1111/j.1502-3885.1988.tb00560.x.

Hughes, A.L.C., Gyllencreutz, R., Lohne, Ø.S., Mangerud, J., Svendsen, J.I., 2016. The last Eurasian ice sheets–a chronological database and time-slice reconstruction, DATED-1. Boreas 45 (1), 1–45. https://doi.org/10.1111/bor.2016.45.issue-110.1111/bor.12142.

Hurrell, J.W., 1995. Decadal trends in the North Atlantic Oscillation: regional temperatures and precipitation. Science 269 (5224), 676–679. https://doi.org/10.1126/science.269.5224.676.

Haapala, J.J., Ronkainen, I., Schmelzer, N., Sztobryn, M., 2015. Recent Change - Sea Ice. In: Team, T.B.I.A. (Ed.), Second Assessment of Climate Change for the Baltic Sea Basin. Regional Climate Studies. Springer International Publishing, Cham, pp. 145–153. https://doi.org/10.1007/978-3-319-16006-1_8.

Hanssen-Bauer, I., Førland, E., 2000. Temperature and precipitation variations in Norway 1900–1994 and their links to atmospheric circulation. Int. J. Climatol.: A J. Royal Meteorolog. Soc. 20 (14), 1693–1708. https://doi.org/10.1002/1097-0088(20001130)20:14<1693::AID-JOC567>3.0.CO;2-7.

IAEA/WMO., 2019. Global Network of Isotopes in Precipitation. The GNIP Database. Available at: https://nucleus.iaea.org/wiser.

Ingraham, N.L., Taylor, B.E., 1991. Light stable isotope systematics of large-scale hydrologic regimes in California and Nevada. Water Resour. Res. 27 (1), 77–90. https://doi.org/10.1029/90WR01708.

Irannezhad, M., Marttila, H., Kløve, B., 2014. Long-term variations and trends in precipitation in Finland. Int. J. Climatol. 34 (10), 3139–3153. https://doi.org/10.1002/joc.2014.34.issue-1010.1002/joc.3902.

Jakobsson, M., Mayer, L., Coakley, B., Dowdeswell, J.A., Forbes, S., Fridman, B., Hodnesdal, H., Noormets, R., Pedersen, R., Rebesco, M., Schenke, H.W., Zarayskaya, Y., Accettella, D., Armstrong, A., Anderson, R.M., Bienhoff, P., Camerlenghi, A., Church, I., Edwards, M., Gardner, J.V., Hall, J.K., Hell, B., Hestvik, O., Kristoffersen, Y., Marcussen, C., Mohammad, R., Mosher, D., Nghiem, S. V., Pedrosa, M.T., Travaglini, P.G., Weatherall, P., 2012. The International Bathymetric Chart of the Arctic Ocean (IBCAO) version 3.0. Geophys. Res. Lett. 39 (12), L12609. https://doi.org/10.1029/2012GL052219.

Jones, M.D., Dee, S., Anderson, L., Baker, A., Bowen, G., Noone, D., 2016. Water isotope systematics: improving our palaeoclimate interpretations. Quat. Sci. Rev. 131 (B), 243–249. https://doi.org/10.1016/j.quascirev.2015.11.014.

Jonsson, C.E., Leng, M.J., Rosqvist, G.C., Seibert, J., Arrowsmith, C., 2009. Stable oxygen and hydrogen isotopes in sub-Arctic lake waters from northern Sweden. J. Hydrol. 376 (1–2), 143–151. https://doi.org/10.1016/j.jhydrol.2009.07.021.

Jonsson, C.E., Rosqvist, G.C., Leng, M.J., Bigler, C., Bergman, J., Tillman, P.K., Sloane, H. J., 2010. High-resolution diatom $\delta^{18}O$ records, from the last 150 years, reflecting changes in amount of winter precipitation in two sub-Arctic high-altitude lakes in the Swedish Scandes. J. Quat. Sci. 25 (6), 918–930. https://doi.org/10.1002/jqs.1372.

Jouzel, J., Merlivat, L., 1984. Deuterium and oxygen 18 in precipitation: Modeling of the isotopic effects during snow formation. J. Geophys. Res.: Atmos. 89 (D7), 11749–11757. https://doi.org/10.1029/JD089iD07p11749.

Jutebring Sterte, E., Lidman, F., Lindborg, E., Sjöberg, Y., Laudon, H., 2021. How catchment characteristics influence hydrological pathways and travel times in a boreal landscape. Hydrol. Earth Syst. Sci. 25 (4), 2133–2158. https://doi.org/10.5194/hess-25-2133-2021.

Jaagus, J., 2009. Regionalisation of the precipitation pattern in the Baltic Sea drainage basin and its dependence on large-scale atmospheric circulation. Boreal Environ. Res. 14, 31–44.

Katrantsiotis, C., Norström, E., Smittenberg, R.H., Salonen, J.S., Plikk, A., Helmens, K., 2021. Seasonal variability in temperature trends and atmospheric circulation systems during the Eemian (Last Interglacial) based on *n*-alkanes hydrogen isotopes from Northern Finland. Quat. Sci. Rev. 273, 107250. https://doi.org/10.1016/j.quascirev.2021.107250.

Kjellman, S.E., Schomacker, A., Thomas, E.K., Håkansson, L., Duboscq, S., Cluett, A.A., Farnsworth, W.R., Allaart, L., Cowling, O.C., McKay, N.P., Brynjólfsson, S., Ingólfsson, Ó., 2020. Holocene precipitation seasonality in northern Svalbard: Influence of sea ice and regional ocean surface conditions. Quat. Sci. Rev. 240, 106388. https://doi.org/10.1016/j.quascirev.2020.106388.

Korhonen, J., 2006. Long-term changes in lake ice cover in Finland. Hydrol. Res. 37 (4–5), 347–363. https://doi.org/10.2166/nh.2006.019.

Kortelainen, N.M., Karhu, J.A., 2004. Regional and seasonal trends in the oxygen and hydrogen isotope ratios of Finnish groundwaters: a key for mean annual precipitation. J. Hydrol. 285 (1–4), 143–157. https://doi.org/10.1016/j.jhydrol.2003.08.014.

L'Abée-Lund, J.H., Vøllestad, L.A., Brittain, J.E., Kvambekk, Å.S., Solvang, T., 2021. Geographic variation and temporal trends in ice phenology in Norwegian lakes during the period 1890–2020. Cryosphere 15 (5), 2333–2356. https://doi.org/10.5194/tc-15-2333-2021.

Lawrence, Z.D., Perlwitz, J., Butler, A.H., Manney, G.L., Newman, P.A., Lee, S.H., Nash, E.R., 2020. The remarkably strong Arctic stratospheric polar vortex of winter 2020: Links to record-breaking Arctic oscillation and ozone loss. J. Geophys. Res.: Atmos. 125 (22), e2020JD033271 https://doi.org/10.1029/2020JD033271.

LeGrande, A.N., Schmidt, G.A., 2006. Global gridded data set of the oxygen isotopic composition in seawater. Geophys. Res. Lett. 33 (12) https://doi.org/10.1029/2006GL026011.

Leng, M.J., Anderson, N.J., 2003. Isotopic variation in modern lake waters from western Greenland. Holocene 13 (4), 605–611. https://doi.org/10.1191/0959683603hl620rr.

Leng, M.J., Marshall, J.D., 2004. Palaeoclimate interpretation of stable isotope data from lake sediment archives. Quat. Sci. Rev. 23 (7–8), 811–831. https://doi.org/10.1016/j.quascirev.2003.06.012.

Linderholm, H.W., Nicolle, M., Francus, P., Gajewski, K., Helama, S., Korhola, A., Solomina, O., Yu, Z., Zhang, P., D'Andrea, W.J., 2018. Arctic hydroclimate variability during the last 2000 years. Clim. Past 14 (4), 473–514. https://doi.org/10.5194/cp-14-473-2018.

Lombino, A., Atkinson, T., Brooks, S.J., Gröcke, D.R., Holmes, J., Jones, V.J., Marshall, J. D., 2021. Experimental determination of the temperature dependence of oxygen-isotope fractionation between water and chitinous head capsules of chironomid larvae. J. Paleolimnol. 66 (2), 117–124. https://doi.org/10.1007/s10933-021-00191-z.

Laasanen, O., 1982. *Vesistöjen jäätymis-, jäänlähtö-, jäänpaksuus-ja pintaveden lämpötilatilastoja. Freeze-up, break-up, ice thickness and surface water temperature statistics in lakes and rivers in Finland*: Vesihallitus. National Board of Waters, Finland. Publ. Water Res. Inst. 77, 68 pp.

MacDonald, L.A., Wolfe, B.B., Turner, K.W., Anderson, L., Arp, C.D., Birks, S.J., Bouchard, F., Edwards, T.W.D., Farquharson, N., Hall, R.I., McDonald, I., Narancic, B., Ouimet, C., Pienitz, R., Tondu, J., White, H., 2017. A synthesis of thermokarst lake water balance in high-latitude regions of North America from isotope tracers. Arct. Sci. 3 (2), 118–149. https://doi.org/10.1139/as-2016-0019.

Marshall, J., Kushnir, Y., Battisti, D., Chang, P., Czaja, A., Dickson, R., Hurrell, J., McCartney, M., Saravanan, R., Visbeck, M., 2001. North Atlantic climate variability: phenomena, impacts and mechanisms. Int. J. Climatol.: J. R. Meteorol. Society 21 (15), 1863–1898. https://doi.org/10.1002/(ISSN)1097-008810.1002/joc.v21:1510.1002/joc.693.

Mellat, M., Bailey, H., Mustonen, K.-R., Marttila, H., Klein, E.S., Gribanov, K., Bret-Harte, M.S., Chupakov, A.V., Divine, D.V., Else, B., Filippov, I., Hyöky, V., Jones, S., Kirpotin, S.N., Kroon, A., Markussen, H.T., Nielsen, M., Olsen, M., Paavola, R., Pokrovsky, O.S., Prokushkin, A., Rasch, M., Raundrup, K., Suominen, O., Syvänperä, I., Vignisson, S.R., Zarov, E., Welker, J.M., 2021. Hydroclimatic controls on the isotopic ($\delta^{18}O$, δ^2H, *d-excess*) traits of pan-Arctic summer rainfall events. Front. Earth Sci. 9, 651731 https://doi.org/10.3389/feart.2021.651731.

MET Norway, 2021. seKlima. Norwegian Meteorological Institute. Available at: https://klimaservicesenter.no/observations/.

Moen, A., 1998. Vegetasjonsatlas for Norge: Vegetasjon. Norwegian Mapping Authority, Hønefoss, p. 199.

Mügler, I., Sachse, D., Werner, M., Xu, B., Wu, G., Yao, T., Gleixner, G., 2008. Effect of lake evaporation on δD values of lacustrine *n*-alkanes: A comparison of Nam Co (Tibetan Plateau) and Holzmaar (Germany). Org Geochem. 39 (6), 711–729. https://doi.org/10.1016/j.orggeochem.2008.02.008.

National Snow and Ice Data Center, 2019. SOTC: Sea ice. Available at: http://nsidc.org/cryosphere/sotc/sea_ice.html.

National Weather Service Climate Prediction Center, 2021. Arctic Oscillation. Available at: https://www.cpc.ncep.noaa.gov/data.

NGU, 2021. Superficial deposits - National Database. Geological Survey of Norway, Available at: http://geo.ngu.no/kart/losmasse_mobil/.

Nichols, J.E., Walcott, M., Bradley, R., Pilcher, J., Huang, Y., 2009. Quantitative assessment of precipitation seasonality and summer surface wetness using ombrotrophic sediments from an Arctic Norwegian peatland. Quat. Res. 72 (3), 443–451. https://doi.org/10.1016/j.yqres.2009.07.007.

O'Sadnick, M., Petrich, C., Brekke, C., Skarðhamar, J., 2020. Ice extent in sub-arctic fjords and coastal areas from 2001 to 2019 analyzed from MODIS imagery. Ann. Glaciol. 61 (82), 210–226. https://doi.org/10.1017/aog.2020.34.

Palecki, M., Barry, R., 1986. Freeze-up and break-up of lakes as an index of temperature changes during the transition seasons: a case study for Finland. J. Appl. Meteorol.

Climatol. 25 (7), 893–902. https://doi.org/10.1175/1520-0450(1986)025<0893:FUABUO>2.0.CO;2.
Papritz, L., Sodemann, H., 2018. Characterizing the local and intense water cycle during a cold air outbreak in the Nordic seas. Mon. Weather Rev. 146 (11), 3567–3588. https://doi.org/10.1175/MWR-D-18-0172.1.
Putman, A.L., Feng, X., Sonder, L.J., Posmentier, E.S., 2017. Annual variation in event-scale precipitation δ^2H at Barrow, AK, reflects vapor source region. Atmos. Chem. Phys. 17 (7), 4627–4639. https://doi.org/10.5194/acp-17-4627-2017.
Putman, A.L., Fiorella, R.P., Bowen, G.J., Cai, Z., 2019. A global perspective on local meteoric water lines: Meta-analytic insight into fundamental controls and practical constraints. Water Resour. Res. 55 (8), 6896–6910. https://doi.org/10.1029/2019WR025181.
Rach, O., Kahmen, A., Brauer, A., Sachse, D., 2017. A dual-biomarker approach for quantification of changes in relative humidity from sedimentary lipid D/ H ratios. Clim. Past 13 (7), 741–757. https://doi.org/10.5194/cp-13-741-2017.
Rawlins, M.A., Steele, M., Holland, M.M., Adam, J.C., Cherry, J.E., Francis, J.A., Groisman, P.Y., Hinzman, L.D., Huntington, T.G., Kane, D.L., 2010. Analysis of the Arctic system for freshwater cycle intensification: Observations and expectations. J. Clim. 23 (21), 5715–5737. https://doi.org/10.1175/2010JCLI3421.1.
Rosqvist, G., Jonsson, C., Yam, R., Karlén, W., Shemesh, A., 2004. Diatom oxygen isotopes in pro-glacial lake sediments from northern Sweden: a 5000 year record of atmospheric circulation. Quat. Sci. Rev. 23 (7–8), 851–859. https://doi.org/10.1016/j.quascirev.2003.06.009.
Rosqvist, G.C., Leng, M.J., Goslar, T., Sloane, H.J., Bigler, C., Cunningham, L., Dadal, A., Bergman, J., Berntsson, A., Jonsson, C., Wastegård, S., 2013. Shifts in precipitation during the last millennium in northern Scandinavia from lacustrine isotope records. Quat. Sci. Rev. 66, 22–34. https://doi.org/10.1016/j.quascirev.2012.10.030.
Rosqvist, G.C., Leng, M.J., Jonsson, C., 2007. North Atlantic region atmospheric circulation dynamics inferred from a late-Holocene lacustrine carbonate isotope record, northern Swedish Lapland. Holocene 17 (7), 867–873. https://doi.org/10.1177/0959683607080508.
Rozanski, K., Araguás-Araguás, L., Gonfiantini, R., 1993. Isotopic patterns in modern global precipitation. In: Swart, P.K., Lohmann, K.C., Mckenzie, J., Savin, S. (Eds.), Climate Change in Continental Isotopic Records. Geophysical Monograph Series 78, 1-36.
Rozanski, K., Sonntag, C., Münnich, K., 1982. Factors controlling stable isotope composition of European precipitation. Tellus 34 (2), 142–150. https://doi.org/10.1111/j.2153-3490.1982.tb01801.x.
Ruuhijärvi, R., 1983. The Finnish mire types and their regional distribution. In: Gore, A. (Ed.), Mires: swamp, bog, fen and moor, regional studies. Elsevier, Amsterdam, pp. 47–67.
Sachse, D., Billault, I., Bowen, G.J., Chikaraishi, Y., Dawson, T.E., Feakins, S.J., Freeman, K.H., Magill, C.R., McInerney, F.A., van der Meer, M.T.J., Polissar, P., Robins, R.J., Sachs, J.P., Schmidt, H.-L., Sessions, A.L., White, J.W.C., West, J.B., Kahmen, A., 2012. Molecular Paleohydrology: Interpreting the Hydrogen-Isotopic Composition of Lipid Biomarkers from Photosynthesizing Organisms. Annu. Rev. Earth Planet. Sci. 40 (1), 221–249. https://doi.org/10.1146/earth.2012.40.issue-110.1146/annurev-earth-042711-105535.
Schmidt, G.A., Bigg, G.R., Rohling, E.J., 1999. Global Seawater Oxygen-18 Database - v1.22. Available at: https://data.giss.nasa.gov/o18data/.
Seppä, H., 2002. Mires of Finland: Regional and local controls of vegetation, landforms, and long-term dynamics. Fennia-Int. J. Geogr. 180 (1–2), 43–60. https://fennia.journal.fi/article/view/3763.
Shapiro, M., Fedor, L., Hampel, T., 1987. Research aircraft measurements of a polar low over the Norwegian Sea. Tellus A: Dynamic Meteorol. Oceanogr. 39 (4), 272–306. https://doi.org/10.3402/tellusa.v39i4.11761.
Shemesh, A., Rosqvist, G., Rietti-Shati, M., Rubensdotter, L., Bigler, C., Yam, R., Karlén, W., 2001. Holocene climatic change in Swedish Lapland inferred from an oxygen-isotope record of lacustrine biogenic silica. Holocene 11 (4), 447–454. https://doi.org/10.1191/095968301678302887.
Singh, H.K., Bitz, C.M., Donohoe, A., Rasch, P.J., 2017. A source–receptor perspective on the polar hydrologic cycle: Sources, seasonality, and Arctic-Antarctic parity in the hydrologic cycle response to CO_2 doubling. J. Clim. 30 (24), 9999–10017. https://doi.org/10.1175/JCLI-D-16-0917.1.
Sjöfartsverket & SMHI, 2020a. *A Summary of the Ice Season and Icebreaking Activities 2018/2019*. Swedish Maritime Administration and Swedish Meteorological and Hydrological Institute. 55 pp. Available at: https://www.smhi.se/oceanografi/istjanst/havsis_en.php.
Sjöfartsverket & SMHI, 2020b. *A Summary of the Ice Season and Icebreaking Activities 2019/2020*. Swedish Maritime Administration and Swedish Meteorological and Hydrological Institute. 52 pp. Available at: https://www.smhi.se/oceanografi/istjanst/havsis_en.php.
SMHI, 2021. Download meteorological observations. Swedish Meteorological and Hydrological Institute. Available at: https://www.smhi.se/data/meteorologi/ladda-ner-meteorologiska-observationer.
Sodemann, H., Masson-Delmotte, V., Schwierz, C., Vinther, B.M., Wernli, H., 2008. Interannual variability of Greenland winter precipitation sources: 2. Effects of North Atlantic Oscillation variability on stable isotopes in precipitation. J. Geophys. Res. *Atmospheres* 113 (D12). https://doi.org/10.1029/2007JD009416.
St. Amour, N.A., 2009. A multi-proxy study of Holocene atmospheric circulation dynamics recorded in lake sediments in Fennoscandia. PhD Thesis, University of Waterloo, Ontario, Canada. 253 pp. http://hdl.handle.net/10012/4225.
St. Amour, N.A., Hammarlund, D., Edwards, T.W., Wolfe, B.B., 2010. New insights into Holocene atmospheric circulation dynamics in central Scandinavia inferred from oxygen-isotope records of lake-sediment cellulose. Boreas 39 (4), 770–782. https://doi.org/10.1111/j.1502-3885.2010.00169.x.
Steen-Larsen, H.C., Masson-Delmotte, V., Sjolte, J., Johnsen, S.J., Vinther, B.M., Bréon, F.-M., Clausen, H.B., Dahl-Jensen, D., Falourd, S., Fettweis, X., Gallée, H., Jouzel, J., Kageyama, M., Lerche, H., Minster, B., Picard, G., Punge, H.J., Risi, C., Salas, D., Schwander, J., Steffen, K., Sveinbjörnsdottír, A.E., Svensson, A., White, J., 2011. Understanding the climatic signal in the water stable isotope records from the NEEM shallow firn/ice cores in northwest Greenland. J. Geophys. Res.: Atmos. 116 (D6) https://doi.org/10.1029/2010JD014311.
Stroeven, A.P., Hättestrand, C., Kleman, J., Heyman, J., Fabel, D., Fredin, O., Goodfellow, B.W., Harbor, J.M., Jansen, J.D., Olsen, L., Caffee, M.W., Fink, D., Lundqvist, J., Rosqvist, G.C., Strömberg, B., Jansson, K.N., 2016. Deglaciation of Fennoscandia. Quat. Sci. Rev. 147, 91–121. https://doi.org/10.1016/j.quascirev.2015.09.016.
Sundqvist, H.S., Kaufman, D.S., McKay, N., Balascio, N., Briner, J., Cwynar, L., Sejrup, H., Seppä, H., Subetto, D., Andrews, J., 2014. Arctic Holocene proxy climate database–new approaches to assessing geochronological accuracy and encoding climate variables. Clim. Past 10 (4), 1605–1631. https://doi.org/10.5194/cp-10-1605-2014.
Thienemann, M., Kusch, S., Vogel, H., Ritter, B., Schefub, E., Rethemeyer, J., 2019. Neoglacial transition of atmospheric circulation patterns over Fennoscandia recorded in Holocene Lake Torneträsk sediments. Boreas 48 (2), 287–298. https://doi.org/10.1111/bor.2019.48.issue-210.1111/bor.12365.
Thomas, E., Castañeda, I., McKay, N., Briner, J., Salacup, J., Nguyen, K., Schweinsberg, A., 2018. A wetter Arctic coincident with hemispheric warming 8,000 years ago. Geophys. Res. Lett. 45 (19), 10,637–610,647. https://doi.org/10.1029/2018GL079517.
Thomas, E.K., Hollister, K.V., Cluett, A.A., Corcoran, M.C., Briner, J.P., 2020. Reconstructing Arctic precipitation seasonality using aquatic leaf wax δ^2H in lakes with contrasting residence times. Paleoceanogr. Paleoclimatol. 35 (7), e2020PA003886 https://doi.org/10.1029/2020PA003886.
Thompson, D.W., Wallace, J.M., 1998. The Arctic Oscillation signature in the wintertime geopotential height and temperature fields. Geophys. Res. Lett. 25 (9), 1297–1300. https://doi.org/10.1029/98GL00950.
Tondu, J., Turner, K., Wolfe, B., Hall, R., Edwards, T., McDonald, I., 2013. Using water isotope tracers to develop the hydrological component of a long-term aquatic ecosystem monitoring program for a northern lake-rich landscape. Arct. Antarct. Alp. Res. 45 (4), 594–614. https://doi.org/10.1657/1938-4246-45.4.594.
Uvo, C.B., 2003. Analysis and regionalization of northern European winter precipitation based on its relationship with the North Atlantic Oscillation. Int. J. Climatol.: J. R. Meteorol. Soc. 23 (10), 1185–1194. https://doi.org/10.1002/(ISSN)1097-008810.1002/joc.v23:1010.1002/joc.930.
van Geldern, R., Barth, J.A., 2012. Optimization of instrument setup and post-run corrections for oxygen and hydrogen stable isotope measurements of water by isotope ratio infrared spectroscopy (IRIS). Limnol. Oceanogr. Methods 10 (12), 1024–1036. https://doi.org/10.4319/lom.2012.10.1024.
Vázquez, M., Nieto, R., Drumond, A., Gimeno, L., 2016. Moisture transport into the Arctic: Source-receptor relationships and the roles of atmospheric circulation and evaporation. Journal of Geophysical Research: Atmospheres 121 (22), 13,493–13,509. https://doi.org/10.1002/2016JD025400.
Vihma, T., Screen, J., Tjernström, M., Newton, B., Zhang, X., Popova, V., Deser, C., Holland, M., Prowse, T., 2016. The atmospheric role in the Arctic water cycle: A review on processes, past and future changes, and their impacts. J. Geophys. Res. Biogeosci. 121 (3), 586–620. https://doi.org/10.1002/jgrg.v121.310.1002/2015JG003132.
Welker, J.M., 2000. Isotopic (δ^{18}O) characteristics of weekly precipitation collected across the USA: an initial analysis with application to water source studies. Hydrol. Process. 14 (8), 1449–1464. https://doi.org/10.1002/1099-1085(20000615)14:8<1449::AID-HYP993>3.0.CO;2-7.
Weyhenmeyer, G.A., Meili, M., Livingstone, D.M., 2004. Nonlinear temperature response of lake ice breakup. Geophys. Res. Lett. 31, L07203. https://doi.org/10.1029/2004GL019530.
Wrona, F.J., Johansson, M., Culp, J.M., Jenkins, A., Mård, J., Myers-Smith, I.H., Prowse, T.D., Vincent, W.F., Wookey, P.A., 2016. Transitions in Arctic ecosystems: Ecological implications of a changing hydrological regime. J. Geophys. Res. Biogeosci. 121 (3), 650–674. https://doi.org/10.1002/2015JG003133.